A COMPARISON OF AERODYNAMIC MEASUREMENTS OF THE TRANSONIC FLOW THROUGH A PLANE TURBINE CASCADE IN FOUR EUROPEAN WIND TUNNELS

N.C.Baines*, P.I.King, M.L.G.Oldfield
Department of Engineering Science, University of Oxford, Parks Road, Oxford OX1 3PJ, England

R.Kiock, H.Hoheisel, G.Ramm
Institute for Design Aerodynamics, DFVLR, Flughafen, D-3300 Braunschweig, West Germany

F.Lehthaus, F.Kost
Institute for Experimental Fluid Mechanics, DFVLR, Bunsenstrasse 10, D-3400 Goettingen, West Germany

C.H.Sieverding
Von Karman Institute for Fluid Dynamics, Chaussee de Waterloo 72, B-1640 Rhode-St-Genese, Belgium

ABSTRACT

The VKI-1 turbine blade profile has been tested in plane cascades in four European wind tunnels at subsonic and transonic conditions. Measurements included blade surface pressure distributions and wake traverse measurements over ranges of Mach and Reynolds numbers, together with Schlieren photographs. The results from the four tunnels are compared and analysed in the paper. This comparison has enabled deductions to be made about the nature and scale of external influences, including tunnel dimensions and geometry, and the importance of cascade parameters such as axial velocity density ratio. The different measurement techniques employed, their suitability and accuracy, are also discussed, with particular reference to the problems of measurement in the wake region downstream of the cascade.

* Present address: Department of Mechanical Engineering, Imperial College, Exhibition Road, London, SW7 2BX

NOMENCLATURE

c	chord
h	width of test section (blade height, blade span)
H	height of channel perpendicular to the flow direction
M	Mach number: $M_1=f(P_1/P_{01})$, $M_2=f(P_2/P_{02})$, $M_{2,is}=f(P_2/P_{01})$
o	throat
P	pressure
r	radius
Re	Reynolds number: $Re = w\rho c/\mu$
s	spacing
Tu	degree of turbulence: $Tu = 100\sqrt{(w'^2)}/w$
w	velocity
x,y	blade coordinates
β	flow angle (measured from the axial direction)
β_s	stagger angle (measured from the axial direction)
μ	dynamic viscosity
ζ	loss coefficient: $\zeta = 1 - (w_2/w_{2,is})^2$
ρ	density
Ω	axial velocity density ratio: $\Omega = \rho_2 w_2 \cos\beta_2/\rho_1 w_1 \cos\beta_1$

Subscripts

0	stagnation
1	measurement plane upstream of cascade
2	homogeneous exit flow from cascade
ch	choked flow
is	isentropic flow
P	pressure surface
S	suction surface
te	trailing edge

Abbreviations

AVDR	axial velocity density ratio
BS	Braunschweig (DFVLR)
GO	Goettingen (DFVLR)
OX	Oxford (University Engineering Laboratory)
RG	Rhode-St-Genese (Von Karman Institute)

1. INTRODUCTION

Cascade testing has for many years been an important stage in the design and development of new blades for high-speed turbomachines and there is little doubt that it will continue to be used in the future. Historically work has concentrated on two-dimensional flows in plane cascades, although in recent years annular cascades, with or without rotating stages, have been developed which permit the simulation of many three-dimensional effects. Nevertheless, there is still much testing which can usefully be done, and is being done, in plane cascades, for our knowledge of the phenomena occurring even in a simplified two-dimensional flow is still far from complete.

One important example of this is the cascade environment, which includes factors such as the development of the inlet flow, the way in which the cascade exit is constrained or guided by the cascade test section, blockage due to measuring probes, etc., all of which can significantly influence the cascade performance, particularly in the transonic regime. Most of these effects are not well understood and the data have generally been sparse and difficult to correlate. Therefore, an attempt has been made to compare the aerodynamic data obtained on a turbine cascade of given geometry in four different wind tunnels at subsonic and transonic flow conditions in order to gain some insight into the magnitude of such "tunnel effects", and the mechanisms by which they influence the cascade.

Some of the individual cascades were of different sizes due to the special test conditions. The probes used were different in size and shape. The operating conditions were steady as well as intermittent. Flow properties were measured in an upstream plane, along the blade surface and in a downstream plane of the cascade. This work was first reported in [1]. The present paper includes a more full discussion of the results, includes data at additional operating conditions and data taken with other measuring techniques such as a laser anemometer, and makes a preliminary assessment of comparative uncertainties due to measurement and non-periodicities in the flow.

2. THE TEST MODEL

The blade section is typical of a coolable gas turbine high pressure stage rotor. It was designed following Dejc's method [2]. The suction side is derived from one basic lemniscate, while the pressure side is composed of both a circular arc and a lemniscate. The blade is shown in Figure 1. The profile designated "RG" served as a test case for calculation [3] at the occasion of a VKI lecture series in 1973. Since then it has been used by various authors to check their numerical codes, e.g. [4]. Many of these methods are now capable of very good predictions, and it is therefore important to the development of these methods, as much as to experimental techniques, that the current limitations of experimental data be understood.

Later, after the tests described in [3], it was discovered that the blade manufactured to the RG profile had an undesirable flat part of the front pressure surface. The coordinates were modified

and all subsequent blades, i.e. the blades tested at GO, BS and OX, were made according to the modified coordinates which were listed in [1], and are shown in Figure 1.

The cascade parameters are as follows:

$$s/c = 0.71$$
$$\text{arc cos } (o/s) = 67.8 \text{ deg}$$
$$\beta_s = 33.3 \text{ deg}$$
$$\beta_1 = 30 \text{ deg}$$

The GO blades were equipped with a trip wire of 0.05 mm diameter on the suction surface at x/c = 0.6.

The comparisons here are restricted to the design inlet flow angle, $\beta_1 = 30$ deg.

3. EXPERIMENTAL ARRANGEMENTS

The tests were carried out in wind tunnels at VKI, Rhode-St.-Genese, Belgium, DFVLR Goettingen, West Germany, DFVLR Braunschweig, West Germany, and Oxford University, UK. The details of the individual test sections and instrumentation are summarised below.

3.1 Test sections

There are many differences in the types and dimensions of the facilities used, see Figures 2 and 3, and Table 1. The width of the test section, h, ranged from 50 to 300 mm, and the chord, c, from 32.6 to 100 mm. The number of blades was 7 or 10. A comparison of the blades, drawn to the same scale, is shown in Figure 2. All blade surfaces were ground and can be described as hydraulically smooth. The test sections at BS and OX are the same size so that physically the same cascade could be investigated in these two wind tunnels. The ratio of upstream length to tunnel width covered a large range from 3 to 20. The ratio of downstream length to tunnel width ranged from 0.8 to 5. All facilities were equipped with solid parallel end walls. No tailboards were used.

The deviations of the true values of the geometric cascade parameters from the nominal ones were small, and the deviations from blade to blade within one cascade were also small (Table 1).

3.2 Instrumentation

The flow properties such as static pressure, total pressure and flow angle were measured in planes upstream and downstream of the cascade in order to adjust the flow for given Mach and Reynolds number conditions and in order to carry out wake traverse measurements, see Table 2.

Figure 4 shows the probes used for the wake traverse measurements. Finger probes were used at RG, BS and OX so that each finger (single tube or tube combination) measured one flow quantity, except the RG probe where one finger was sensitive to both total pressure and yaw angle. A wedge probe was used at GO. This probe was originally developed for use in supersonic flows.

All of these probes were calibrated carefully. The calibration of such probes for measuring high subsonic and transonic flows is discussed extensively in [8]. The probes were moved stepwise or continuously with very different velocities, so that a wake traverse over one pitch took between 1 and 180 seconds. Because of the short measuring time of 1 second at OX the transducers were installed in the probe holder with a length of approximately 150 mm for the pneumatic tubes. This length ranged from 1.5 m to 6 m in the other tunnels. To calculate the loss coefficients, the local wake data were transferred to a hypothetical plane of homogeneous flow using the conservation laws [9].

The surface pressures were measured by tappings on two central blades. One blade was equipped with tappings on the suction surface and the other with tappings on the pressure surface. The tappings were distributed over two blades in order to allow the installation of as many pressure tubes as possible. The trailing edge tappings were aligned in the direction of the camber line at the trailing edge. In the case of the GO cascade, tappings were overlapped in the regions of leading and trailing edges so that the pressure could be measured on two neighbouring blades within these regions. In the case of the OX cascade, each tapping was connected to an individual transducer. Scanivalves were used at GO and BS, and a mercury multimanometer was used at RG.

For the wake traverses, the instrumented blades were replaced by blank blades at RG and GO.

In addition to probe measurements, the flow field in the exit plane of the cascade at GO was also measured by means of a laser-2-focus velocimeter. This instrument is capable of measuring velocity and direction in a non-intrusive manner, and was used together with a measurement of total temperature in the stagnation chamber upstream of the cascade test section using a thermocouple to derive the exit Mach number traverse in the pitch direction of the cascade. This is further discussed in section 10.2.

4. OVERALL FLOW CONDITIONS

With the exception of BS, all facilities allow testing at supersonic exit Mach numbers, but only at GO were the tests extended into this range, see Table 3. The exit Reynolds number could be varied independently of the exit Mach number in the tunnels at BS and OX only. The relation of Re_2 with M_2 is shown in Figure 5. The tests in the transonic flow region, M_2 = 0.8 - 1.1 were carried out in all tunnels at around $Re_2 = 8 \times 10^5$, but for the lowest values of M_2, $Re_2 = 3.5 \times 10^5$ at RG and GO. For the purposes of comparison at low exit Mach numbers, the Reynolds number at BS was reduced in this region.

The degree of turbulence was not increased artificially, i.e. it was of the order of 1%, and the total temperature in every case was close to ambient, see Table 3.

5. COMPARISON OF RESULTS

The results of cascade measurements in the four tunnels include checks on the inlet flow field, blade surface pressures and exit flow traverses in order to establish the aerodynamic loss and related parameters such as exit flow angle and axial velocity density ratio. Comparisons with a numerical prediction scheme and with laser-2-focus measurements of the wake region are also presented. All of these measurements were made at a fixed (or constrained) Reynolds number, and with a fixed cascade geometry, and so in order to illustrate further the behaviour of this test section, some results for varying Reynolds number and aspect ratio from one of the tunnels are also discussed.

In attempting to draw conclusions from these comparisons, it is important to appreciate the effects of measurement uncertainty and cascade periodicity. On the simplest level these can help to decide whether measured differences between tunnels are of significance or not, while a more fundamental understanding of measurement uncertainties can assist in the development of measuring techniques and measuring instruments, and in the design of future experiments. For this reason an attempt has been made to assign values to these quantities wherever possible. It must be emphasised that any assessment of measurement accuracy is to some extent subjective, for there is no "right" way to quantify it in the absence of a universally agreed scheme (one method, that used for the OX data, is described in [12]), and it should be understood that this condition applies to all of the values quoted in this paper.

The presentation of results is complicated by the fact that the comparison was not a completely controlled experiment. Most of the testing in all the tunnels was done before the idea of doing such a comparison was proposed. It was therefore not possible in many cases to find exactly comparable data, for example, blade surface pressure distributions at precisely the same Mach and Reynolds numbers. The losses and outlet flow angles quoted for RG are not those reported in [3] but data taken in 1980 with a slightly different probe from that used before. These data are believed to be more accurate and are used to present mixed out values, which was not the case for the first data set. The results of GO reported in this paper are evaluated from measurements conducted at the end of 1983. Contrary to the earlier experimental investigations [4] the probe stem and holder were changed in order to decrease blockage, which mainly affected the exit flow angle. Additionally, a new and more accurate probe calibration was used.

6. INLET FLOW FIELD

The inclination of the cascade and the gaps between the end blades and the top and bottom walls were chosen in such a way that the inlet flow angle is very close to 30° and the flow is periodic in the measurement plane upstream and downstream of the cascade. The first two parts of Table 4 shows some of the checks of those flow parameters taken over several pitches. The data shown in Table 4 are the inlet Mach number and flow angle, each given as a magnitude and, where possible, estimates of the

accuracy of measurement and of the variation over a number of pitches. The latter quantity is a measure of the periodicity of the cascade. The measurement accuracy values take account of effects such as probe calibration and setting errors, transducer calibrations, and any random variations of the inlet flow with time. No measurements of inlet flow angle are available from BS because the inlet settings are known well from experience, and this check is not made.

The inlet Mach number generally reaches its maximum when the local Mach number across the blade passage exceeds unity. This choking condition results in an exit Mach number of roughly unity. Figure 6 shows different levels for inlet Mach number in the four facilities. For comparison, the theoretical values for choked, two-dimensional flow and for a straight sonic line are indicated for the nominal and for the true geometry of all four cascades. These two values are very close to each other. There is, however, marked differences between some of the measured and the theoretical values, and between the measured values themselves, which cannot be accounted for simply by experimental uncertainty and periodicity limitations.

In the absence of endwall boundary layers the choking Mach number will be lower than the theoretical value because of the blade boundary layers and the curvature of the sonic line. In the presence of endwall boundary layers the flow acceleration between the cascade inlet and throat planes produces an effective increase of channel width and hence higher inlet Mach numbers, as can be seen for all the tunnels except OX in Figure 6. This effect is proportionally larger for longer inlet ducts, in which the upstream boundary layers on the endwalls have longer in which to grow, and larger for smaller channel widths, in which the endwall boundary layers occupy a greater fraction of the duct width. Evidence in favour of this argument is shown in Table 5, where it can be seen that for the four tunnels inlet Mach number correlates with a composite parameter (inlet channel length/inlet duct width).

7. BLADE SURFACE MACH NUMBER DISTRIBUTIONS

Comparisons of Mach number distributions at two flow conditions are shown here: one example for pure subsonic flow and one in the transonic flow region, see Figures 7 and 8. In each case the flow is characterised by acceleration along the suction surface up to x/c = 0.6 and by moderate deceleration downstream.

In the subsonic case the exit Mach numbers in the four facilities lie close together, forming a band of $\Delta M_2 = 0.006$, but the blade surface Mach number distributions differ considerably in the rear half of the suction surface. The Reynolds number variation between 7 and 9 x 10^5 does not account for this (see section 9.4). Experimental accuracies are likely to be of similar magnitudes to those of M_1 and M_2 listed in Table 4, so that these too cannot account for the whole of the difference.

Figure 7 shows that in particular the Mach number values of OX are significantly higher than those of BS despite the identical cascade hardware and the lower inlet Mach number (Figure 6). This

difference is observed at other exit Mach numbers, and is believed to be due to a discrepancy in the measurement of exit static pressure. Whereas the BS cascade exhausts into a plenum, the OX cascade exhausts through a duct containing the probe traversing mechanism and then to the exhaust system. The practice at OX was formerly to calibrate a static pressure tapping in the sidewall of this duct behind a sudden expansion step against the mixed out static pressure measured with the probe in order to be able to set up for predetermined Mach and Reynolds numbers when the probe is removed. This would be done for measuring blade surface velocities, which it is known that the probe can influence. It is apparent from both Figures 7 and 8 that there is a significant loss in pressure due to the presence of the probe and its traverse mechanism while calibrating, despite every effort to minimise their dimensions. From these and other results at OX it was concluded that a more representative downstream static pressure can be based on the average of several sidewall tappings covering one or more pitches in the plane of the probe tip, where the effects of probe blockage are much reduced.

This effect of blockage, and the general problems of measuring representative static pressures in the exit of a cascade where there are wakes, large spatial pressure gradients and in transonic flows also shock waves, is a serious one, and is probably worse in the case of tunnels such as OX where the exhaust duct is relatively restricted, than for BS, for example, where the exhaust is into a large plenum at an effectively constant static pressure.

The results at GO, BS and RG agree fairly well. The slightly higher Mach numbers for the RG blade in the front part of the pressure and suction surfaces are related to a different blade contour. This is illustrated in Figure 1 and has been checked on a Zeiss profile measuring machine. The difference has also been reproduced computationally, see section 8 and reference [4].

In the transonic flow case, Figure 8, sonic conditions are obtained at about $x/c = 0.47$ on the suction side and $x/c = 0.99$ on the pressure side, resulting in a fairly straight sonic line across the blade passage. A comparison of the four Mach number distributions leads to similar conclusions as in the subsonic case. In particular, the Mach number distribution for the RG blade indicates a turbulent shock boundary layer interaction. The surface roughness, due to the very dense instrumentation on a small blade, or possibly a different structure of the freestream turbulence, might be responsible for transition near the throat. However, the band of exit Mach numbers is wider with $\Delta M_2 = 0.027$, and this may influence the location of compression shocks. Heavy decelerations occur in the suction side at $x/c = 0.65$ and 0.98. The schlieren picture from GO in Figure 9 shows compression shocks at these two locations.

The trends shown in the transonic case continue into the region of supersonic exit Mach numbers. As the exit Mach number increases, the shock impinging on the suction surface boundary layer becomes stronger, and the combined effect of this and the rapid deceleration required thereafter causes a separation bubble to form. Three schlieren photographs from GO at exit Mach numbers

of 1.050, 1.133 and 1.159, and the corresponding blade surface pressure distributions, are shown in Figures 10 and 11. A growing laminar separation bubble, which at the highest Mach number occupies a region extending almost to the trailing edge, and the shock-boundary layer interaction, are clearly visible. This results in a very large increase in loss at supersonic exit Mach numbers (section 9), and has the unfortunate effect of making this blade quite unsuitable for comparison purposes in this region.

The trip wire on the GO blade at x/c = 0.60 was an attempt to control this separation by inducing an early transition of the boundary layer. However, it appears to have been ineffective (presumably the wire was too thin), since the shock boundary layer interaction downstream of the trip wire at high Mach numbers is still characteristic of a laminar separation. There is evidence that transition may occur naturally at about the point of minimum static pressure at this high Reynolds number. Some further discussion of this point, including results at lower Reynolds numbers, is given in section 9.4. The effect of the trip wire can be seen from the Mach number distributions in Figures 7 and 9 in particular to be very localised. Recent tests at GO without the trip wire have demonstrated that the effect of the wire is indeed confined to this small region of the blade surface.

8. NUMERICAL PREDICTIONS OF BLADE SURFACE MACH NUMBER

This paper is principally concerned with the comparison of experimental data from the four wind tunnels. The VKI-1 blade profile has, however, become a standard test case for numerical prediction techniques, so that it is appropriate to say a few words here about such predictions, using as an example a two-dimensional, inviscid, time-marching scheme. A more complete discussion, including the details of the numerical model, is to be found in reference [4].

The blade surface pressure distributions measured at RG and GO for the two cases shown in Figures 7 and 8 are reproduced in Figures 12 and 13, together with the corresponding theoretical curves. In each case the predictions were done using the actual blade profiles, and the effects of differences in the profiles on the forward parts of the pressure and suction surfaces are well reproduced.

On the rear part of the suction surface beyond the point of maximum Mach number there is a stronger initial diffusion on the RG than the GO blade. At the higher Mach number there is a laminar shock boundary layer interaction at about x/c = 0.6 on the GO blade, whereas the RG blade with the earlier transition has a turbulent shock boundary layer interaction. Clearly only those prediction schemes which have some ability to model the viscous boundary layer will be able to cope with this kind of phenomenon. This emphasises the point that test cases should be chosen with great care and understanding, and that the actual, rather than the nominal, blade profile should always be used.

9. INTEGRATED WAKE TRAVERSE RESULTS

In all four tunnels the cascade wakes were traversed with a probe measuring the local static pressure, total pressure and flow angle. These data were then integrated to produce mixed-out values of the parameters, from which the enthalpy loss coefficient and the axial velocity density ratio were also calculated. In each case the measurements and integration were done over a number of pitches, given for each tunnel in Table 4.

9.1 Loss coeffients

The loss coefficients are presented as a function of exit Mach number in Figure 14. For exit Mach numbers less than 0.95 the loss coefficient is nearly constant. The higher loss at the lowest Mach numbers at RG and GO is due to the lower Reynolds numbers in these two cases (see section 9.4). For exit Mach numbers between about 0.80 and 0.95, however, the Reynolds numbers are very similar. In this region the RG, GO and BS data differ by only $\Delta\bar{\xi} = 0.003$, and this is within the bounds of the pitchwise variation of the data, as shown in Table 4. The scatter in the OX losses is somewhat higher. However, the combined effects of pitchwise variation and measurement uncertainty bring the data points within the limits of scatter of the other three tunnels (Figure 15). It should be remembered that the OX facility is a short-duration tunnel which requires the use of instrumentation with a relatively fast response. This instrumentation detects random time-varying flow unsteadiness which adds to the measurement uncertainty, but which is not detected by the much slower response instrumentation of the other tunnels. The consequences of this will be seen when the local wake traverse data are considered below in section 10.1.

The influence that the flow separation and shock waves at high Mach numbers has on the loss coefficient can be clearly seen in Figure 14 at supersonic exit Mach numbers. The data here (from GO only) exhibit considerable scatter because of the unsteadiness of this phenomenon, and so are shown as a band as well as discrete data points.

The effect of scatter on the GO data are shown further in Figures 16 and 17, where error bars and regions show the standard deviations in both loss and exit Mach number measured over a number of pitches. These two figures show the effect of the trip wire, which, although it was not successful in removing the separation at high Mach numbers, significantly reduced the scatter on the data, particularly at low Mach numbers. A tentative conclusion from this might be that natural transition occurs at a slightly different point on each blade in the cascade, resulting in a slightly different loss and hence a larger standard deviation between losses. The effect of the trip wire on the mean value (averaged over all the measured blades) is not significant, as Figure 18 shows. This may not be true of a larger trip wire, however. It is noteworthy that had the loss coefficient values for the untripped rather than the tripped blade been used for the comparison shown in Figure 14 the agreement between the RG, BS and GO tunnels would have even better.

9.2 Exit flow angle

The exit flow angle increases slightly with increasing exit Mach number up to M_2 = 0.95 which corresponds to the low loss region, see Figure 19. In transonic flow the results of RG, GO and BS form a very narrow band of β_2 = 67.2° ± 0.2° which again is within the band of pitch variation in Table 4. This is also consistent with the theoretical value $\beta_{2\,is}$ = 67.8° at M_2 = 1.0, allowing a few tenths of a degree for frictional effects. The theoretical value is calculated using the conservation equations and assuming choked flow and a straight sonic line. The magnitude of β_2 decreases with increasing exit Mach number at M_2 > 1.0 because of the effect of supersonic turning, but in this case the effect is enhanced by the increase in loss mentioned above. This is the reason for the increasing difference in the exit flow angles of isentropic and real flow.

The flow angles measured at OX are about 0.5° higher than those of the other tunnels. This time the combined effects of measurement uncertainty and blade-to-blade variation are insufficient to account for this difference (Table 4). It is possible that the constraining influence of the exit duct of the OX tunnel is sufficient to cause this difference. Another possibility is that the OX probe has recently been recalibrated, and the new calibration relative to the old shows a shift in angle of similar magnitude, but it has not been possible to re-test the VKI-1 cascade to check this effect.

Figures 20 and 21 show that the effect of pitch variations on the flow angle measurements are very small for exit Mach numbers less than 0.95. These data are from GO, but as Table 4 shows, the scatter from the other tunnels are likely to be at least as small. In this case the trip wire has very little effect on either the variation between blades or the mean values (Figure 22).

9.3 Axial velocity-density ratio

A check on the flow conditions in the inlet and exit measurement planes can be made by the consideration of the axial velocity density ratio, see Figure 23, which is based on mid-span measurements. A deviation of AVDR from unity may be the result of either a non-two-dimensional flow or a measurement inaccuracy, in particular in the flow angles β_1 and β_2. A measurement error of ±0.5° results in a $\Delta\Omega$ of ±0.005 for an error in β_1 and ±0.02 for an error in β_2. Other parameters such as inlet and exit pressures have a smaller, but still significant, influence.

According to this argument, the effect of differences in measured exit angle shown in Figure 18 should be a difference of ±0.02 in the worst case for values measured in the four tunnels. In fact Figure 23 shows that the difference is 0.08. This can only be accounted for by the inlet conditions, and the fact that the measured inlet Mach numbers for a choked cascade are equal to or greater than the theoretical value, and their magnitudes are in inverse order to the AVDRs, bears this out. Since the inlet Mach numbers are related directly to the ratio of inlet to throat

areas, it follows that the flow downstream of the throat is essentially two-dimensional. If this were not the case, it would be difficult to explain the good agreement in exit flow angle between RG and GO on the one hand and BS on the other. It appears therefore that contrary to compressor cascades non-unity values of AVDR do not necessarily affect the outlet flow angle measurements or the loss measurements (at least at small angles of incidence).

The cumulative effect of measurement uncertainties on AVDR is in fact considerable. Taking into account the effects of inlet and exit flow angle, static and total pressure measurement errors and summing them by the methods set out in [12], the OX result is shown in Table 4 and Figure 24. It can be seen that this far outweighs the effect of non-periodicity. Even so, and assuming that similar results apply to the other tunnels, this effect is unlikely to account for all of the variation seen in Figure 23 and does not negate the previous argument.

Further evidence of the influence of exit flow angle measurement on AVDR comes from the comparison of tripped and untripped blades done at GO. Figure 25 shows that the differences in AVDR mirror quite well, and amplify in magnitude, the differences in measured exit flow angle shown in Figure 22.

9.4 Effect of Reynolds number and aspect ratio

It has been shown that the transonic tests were carried out in the four tunnels at Reynolds numbers around $Re_2 = 8 \times 10^5$. Surface Mach number distributions from the BS tunnel verify that they are influenced by Reynolds number very little for $Re_2 = 3$ to 8×10^5 with a constant exit Mach number of 0.91, see Figure 26. Measurements of the suction surface boundary layer using a flattened pitot probe [11] yielded the following results. In the case of an exit Reynolds number of 3×10^5, bubble transition takes place from 0.60 to 0.65 by interaction of the laminar boundary layer and a compression shock, and the turbulent boundary layer separates at $(x/c)_S = 0.9$. At the higher Reynolds number of 8×10^5, the bubble no longer exists, and transition is assumed to occur at the location of the incident shock, $(x/c) \simeq 0.6$. The turbulent boundary layer remains attached until the trailing edge.

The influence of exit Reynolds number on inlet Mach number and on the wake traverse data is shown in Figure 27. The loss coefficient takes a maximum at $Re_2 = 3 \times 10^5$ because of the existence of the bubble, an extended turbulent boundary layer and turbulent trailing edge separation. Moreover, the inlet Mach number and the wake parameters shown in Figure 27 for a constant exit Mach number are not affected by the Reynolds number in the range $Re_2 = 7$ to 9×10^5.

The low Mach number tests of RG and GO reported in [1] were carried out at a lower Reynolds number of around 3.5×10^5. The higher losses in these cases are in fact due to the reduced Reynolds number and are caused by friction effects. This can be seen in the loss variation with Reynolds number in Figure 27 for an exit Mach number of 0.39. The blade surface Mach number dis-

tribution in Figure 26 does not show any influence of Reynolds number for this Mach number.

The four tunnels have aspect ratios of h/c = 1.53 to 3.00. Tests in the BS tunnel show that the aspect ratio affects the pressure distribution and the wake measurements very little over the ranges of Reynolds and Mach numbers considered, see Figures 27 and 28.

10. LOCAL WAKE TRAVERSE MEASUREMENTS

10.1 Comparison of measurements from the four tunnels

In an attempt to gain some further understanding of the reasons for the differences in the wake traverse parameters between the four tunnels the raw data were examined and were plotted as local values of loss coefficient $\bar{\zeta}$, exit Mach number M_2 and exit flow angle β_2 as functions of pitch position. These parameters, unlike those presented above, are based on upstream flow conditions and local wake traverse measurements at single points in space without any averaging or integration over whole wakes. As nearly comparable overall Mach and Reynolds number conditions conditions were chosen, these being $M_2 \simeq 0.9$ and $Re_2 = 8 \times 10^5$. These are not necessarily the same conditions as those listed in Table 4. In each case several adjacent wakes were analysed in order to assess periodicity more comprehensively than is presented in Table 4. It is unfortunately very difficult to reduce a concept such as periodicity to a few precise and easily understood parameters, so that the standard deviations over several wakes in Table 4 is the only qualitative assessment which is made here.

For RG and GO it was possible to plot values over three wakes at this condition and for OX two wakes (this being limited by the regulated running time of the tunnel). At BS the only example of measurements over several pitches is at an exit Mach number of 0.83, so this condition is plotted together with the data from the other tunnels at the higher Mach number in Figures 29 - 31, and for comparison the one pitch of data at $M_2 = 0.91$ from BS is shown in Figure 32. These figures show the local values of loss coefficient, exit Mach number and exit flow angle as a function of pitch position, together with the mixed out values calculated for each pitch.

Both the absolute and relative distances from the blade trailing edges to the probe traverse plane are listed in Table 2. In Figure 29 the amplitude of the loss coefficient variation at GO is seen to be significantly larger than those of the other three tunnels, which are all very similar. At the greater axial distance of RG it would be expected that more mixing would have taken place, resulting in the shallower and broader wakes which are observed, but this does not account for the BS and OX data which were measured at a slightly smaller relative axial distance than GO. One parameter which is very similar for RG and GO but quite different for BS and OX is the axial length (as a multiple of the chord) of the sidewall before a step expansion behind the cascade exit (see Figure 3). The end of the sidewall at the step expansion imposes a uniform static pressure boundary at this

point, and it is possible that the relative closeness of this boundary at BS and OX is responsible for a faster mixing process in the case of these two tunnels. Certainly there appears to be little justification for attributing this effect to the trip wire on the suction surface of the GO blade, which, if it has any effect at all, causes an early transition and a longer length of turbulent boundary layer.

In Figure 30 the local exit Mach number data are consistent with the local loss coefficients, with less mixing having taken place in the GO tunnel. The OX tunnel shows poorer periodicity in the local measurements, but not in the integrated parameters for each wake as shown in Table 4, and this suggests that the local results are affected primarily by time-varying flow unsteadiness which is random in nature and is, in effect, smoothed by the integration process. It should also be said that the OX tunnel was, at this time, operating at the lower Reynolds number limit of its range (improved operating procedures have now extended this) and the time during which the flow was regulated and valid measurements were possible was severely limited.

Comparing these and the local flow angle measurements shown in Figure 31, the BS and GO results in particular show a consistent pattern of flow angle variation through the wake, with a smaller angle than the freestream value on the pressure side of the wake, the same value as the freestream in the centre and a larger value on the suction side. This is consistent with the freestream flow moving into and filling the low-momentum wake as the mixing progresses. The variations in the other two tunnels are not as clear as this, however.

10.2 Comparison of L2F measurements

The laser anemomenter, either in its Doppler (LDA) or transit (L2F) forms, has been in existence for some years and has been widely used in a variety of applications, although not to any great extent in routine cascade testing. It offers one great advantage in that it is non-intrusive, but since it provides a measure of the local flow velocity (magnitude and direction) only, an additional measurement is required to define the flow completely. In the present case the laser measurements were combined only with the total temperature, measured by means of a thermocouple located upstream of the cascade, in order to calculate the Mach number and flow direction. The assessment of losses, for example, would also require the knowledge of pressure. For the measurements at GO the system developed by Schodl [10] was used.

A comparison of the local exit Mach number and exit angle distributions for probe and L2F measurements are shown in Figures 33 and 34 for a high subsonic Mach number. Outside of the wakes the agreement in Mach number is very good, and the general picture of the pitch-wise variation supports the probe measurements, but within the wakes the probe measures considerably smaller minima. In fact the high level of turbulence recorded inside the wakes (12 - 15% as compared with about 2% in the freestream) may have meant that the time taken in making the L2F measurements was insufficient to produce completely reliable

data. A further possibility is inadequate seeding in the wake regions. Further work is currently in progress at GO to develop this technique.

The flow angles measured by the two methods differ by between 0.5 and 1 degree, although not in a completely systematic way. The accuracy of the L2F measurement is (according to Schodl) of the same order as the probe measurement (Table 4), so that the combined uncertainties may account for the difference.

One final point to note is that the ratio of measuring times by the two methods was about 20:1 in favour of the probe. Laser measurements are therefore substantially more expensive, and with the existing technology are almost certainly impossible in transient tunnels such as that at OX.

11. CONCLUSIONS

A plane turbine cascade using the VKI-1 blade profile was investigated in four European wind tunnels at subsonic and transonic velocities. Due to the different size of the individual test sections, the chord length of the blades ranged from 32.6 to 100 mm. Two of the facilities (OX and BS) were characterised by two particular features: first, they have the same size of test section so that the identical cascade could be investigated, and second, the exit Mach number could be varied at constant Reynolds number. One of the tunnels (OX) was a short-duration type using essentially transient testing techniques, the others were continuous running tunnels. All tests were carried out at normal wind tunnel turbulence. The testing encompassed measurement of the inlet flow field, blade surface static pressures and the exit flow field.

The inlet Mach number evaluated from static and total pressures measured upstream of the cascade is, for a choked cascade, equal to or higher than the theoretical value based on geometric inlet and throat areas, due to the inlet flow displacement by the side wall boundary layers. This may be correlated with the different tunnel inlet geometries.

The surface Mach number distributions show small differences due to small deviations in the contours. Other differences are due to non-identical operating conditions, apart from which the data agree within the likely accuracy of measurement. The cascade operating condition is determined by the total pressure upstream and the static pressure downstream, and the latter in particular must be evaluated very carefully to avoid problems such as probe blockage.

At exit Mach numbers between 0.80 and 0.95 the loss coefficients lie within a band limited by the experimental accuracy of measurement and the blade-to-blade variation. For the continuous tunnels this is 0.040 ± 0.003. The fast response instrumentation used in the short-duration tunnel records random time-varying unsteadiness in the flow which affects the accuracy of mean measurement in this tunnel. At lower Mach numbers there are variations in the measured loss due to different Reynolds numbers, and at higher Reynolds numbers the blade suffers from a

large separation on the suction surface which results in a large increase in loss.

The axial velocity density ratio indicates a nearly two-dimensional flow in only two facilities. The other two tunnels give significantly lower values. The exit flow angles are, however, in good agreement, and this indicates that it is the inlet rather than the exit conditions which are responsible for the differences in AVDR. It appears that a non-unity value of AVDR, at least as long as it is in the range 0.9 - 1.0, does not affect the loss or exit flow angle measurement in a turbine cascade. The accuracy of AVDR measurement is highly sensitive to measurement errors in the data, particularly inlet and exit flow angles.

The wake traverse data, plotted as a function of distance in the pitchwise direction, show good periodicity in the case of the three continuous tunnels. In the short-duration tunnel the periodicity appears to be less good, but the blade-to-blade variation in the integrated parameters is comparable with that in the other tunnels, which indicates that a random flow unsteadiness is present which the integrating process removes. A comparison of the curves from the various tunnels shows that there are significant differences in the rate at which the wakes mix out, and it is suggested that the rate of mixing is influenced by the distance downstream of the cascade the constant static pressure boundary condition imposed by a step expansion in area occurs.

Some measurements in the wake traverse plane of one cascade have been made with a laser-2-focus velocimeter for comparison with the probe measurements. Agreement is generally good except in the centre of the wakes where the turbulence level is very high. This work is continuing.

The VKI-1 profile is much used as a test case for numerical flowfield prediction schemes. It has been demonstrated that the differences in profile between the various tunnels have significant effects on the experimental results which are reproducible numerically. It is therefore important to use actual rather than nominal profiles for comparisons. One profile tested exhibited an early transition on the suction surface, which is thought to be caused by imperfections around the pressure tappings. At high Mach numbers this results in a turbulent shock boundary layer interaction, whereas in the other tunnels a laminar shock boundary layer interaction is observed. In making comparisons with theoretical predictions care must be taken to observe and understand effects such as this.

REFERENCES

[1] Kiock, R., Lehthaus, F., Baines, N.C. and Sieverding, C.H., "The transonic flow through a plane turbine cascade as measured in four European wind tunnels", ASME Paper 85-IGT-44, International Gas Turbine Symposium and Exposition, Beijing, China, 1985.

[2] Dejc, M.E., Filippov, G.A. and Lazarev, L.A., "Atlas of axial turbine blade characteristics". Part 1: Method of profiling and the aerodynamic characteristics of cascades. Moskow, Mashinostroenie Publishing House, 1965, C.E. Trans. 4563.

[3] Sieverding, C.H. "Experimental data on two transonic turbine blade sections and comparison with various theoretical methods", in "Transonic flows in turbomachinery", VKI LS 59, 1973.

[4] Lehthaus, F., "Berechnung der transsonischen Stroemung durch ebene Turbinengitter nach dem Zeit-Schritt-Verfahren", VDI-Forschungsheft 586, 1978, pp.5-24.

[5] Heinemann, H.-J., "The test facility for rectilinear cascades (EGG) of the DFVLR", DFVLR IB 222-83 A 14, 1983.

[6] Hoheisel, H. and Kiock, R., "Zwanzig Jahre Hochgeschwindigkeits-Gitterwindkanal des Instituts fur Aerodynamik der DFVLR in Braunschweig", Zeitschrift fur Flugwissenschaften und Weltraumforschung, Vol.1, No.1, 1977, pp.17-29.

[7] Baines, N.C., Oldfield, M.L.G., Jones, T.V., Schultz, D.L., King, P.I. and Daniels, L.C., "A short duration blowdown tunnel for aerodynamic studies on gas turbine blading", ASME Paper 82-GT-312, 1982.

[8] Sieverding, C.H., "Pressure probe measurements in cascades", in "Modern methods of testing rotating components of turbomachines (instrumentation)", ed. M. Pianko, AGARDograph No.207, 1975.

[9] Amecke, J., "Anwendung der transsonischen Ahnlichkeitsregel auf die Stroemung durch ebene Schaufelgitter", in "Probleme der transsonischen Stroemung durch Turbinenschaufelgitter", VDI-Verlag Duesseldorf, 1970, pp.16-28.

[10] Schodl R., "Laser dual-beam methods for flow measurements in turbomachines", ASME Paper 74-GT-157, 1974.

[11] Schlichting, H., "Boundary layer theory", 7th edition, McGraw-Hill, 1979, pp. 454-5.

[12] Baines, N.C. "Measurement uncertainty in aerodynamic cascade testing", Imperial College Mechanical Engineering Dept. Report, 1986.

Tunnel	RG	GO	BS	OX
Name of facility	High speed cascade wind tunnel (C-2)	Plane cascade wind tunnel (E66)	High speed cascade wind tunnel (HGB)	O.U.E.L. blowdown tunnel
Reference	[3]	[5]	[6]	[7]
Type of facility	Blowdown	Down-draught	Closed loop	Blowdown
Test section $h \times H_1$	50 mm x 160 mm	125 mm x 353 mm	300 mm x 427 mm	300 mm x 420 mm
Length of upstream straight end wall [(1)]	1000 mm	2550 mm	1550 mm	800 mm
Length of downstream guided flow [(2)]	200 mm	650 mm	250 mm	290 mm
Number of blades	10	10	7	Identical with BS cascade
Diff. nom. and real profile [(3)]	±0.031 mm ±0.031 mm	±0.025 mm ±0.040 mm	±0.055 mm ±0.083 mm	
Chord, c	32.6 mm	40 mm	100 mm	
Aspect ratio h/c	1.534	2.083	3.000	
True gauging angle arc cos (o/s) [(4)]	67.74±0.10°	67.92±0.11°	67.96±0.03°	
True pitch [(4)]	23.15±0.04 mm	42.58±0.19 mm	70.88±0.10 mm	
True stagger	33.14±0.09°	33.56±0.12°	33.29±0.03°	

(1) Upstream of cascade centre
(2) Downstream of cascade centre in isentropic exit flow direction $\beta_{2,is} = 67.8°$, range with channel width equal to blade height
(3) Average value and standard deviation around the blade normal to contour, front part of pressure side not considered
(4) Average value and standard deviation over four central pitches

Table 1 Geometric parameters of test sections and cascades

Tunnel	RG	GO	BS	OX
Flow quantities at inlet:				
Static pressure	Side wall tappings	Side wall tappings	Side wall tappings	Side wall tappings
Total pressure	} Probe	} Probe	Probe	} Probe
Flow angle			Not measured	
Flow quantities at exit:				
Static pressure	} Two-finger	} Wedge probe	} Three-finger	} Three-finger
Total pressure	probe		probe	probe
Flow angle				
Wake traverse on blade no. (1)	5	5	4	4
Axial distance (2)	21 mm	27 mm	40 mm	40 mm
Axial distance (2) /chord	0.644	0.45	0.40	0.40
Probe motion	Continuous	Continuous	Step-wise	Continuous
Time required for one wake traverse (3)	45 s	70 s	180 s	1 s
Pressure-tapped blades	5,6	4,5	3,5	3,5

(1) Smooth blade with no pressure tappings in each case
(2) Between trailing edge plane and probe tapping for total pressure measurement
(3) Without flow adjustment

Table 2 Measurement of flow quantities

Tunnel	RG	GO	BS	OX
Cascade exit velocity	Sub/transonic	Sub/supersonic	Sub/transonic	Sub/transonic
Reynolds number Re_2	Varying with exit velocity		Independent of exit velocity	
Turbulence, Tu_1	1%	1%	0.3 - 0.6%	<1%
Total temperature	278 K	290 K	313 K	287 K

Table 3 Operating conditions

Tunnel	RG	GO	BS	OX
Inlet flow conditions:				
M_1 magnitude	0.282	0.282	0.260	0.252
accuracy (±)		0.003		0.003
pitch variation (±)	0.003 (4)	0.001 (4)	0.000 (3)	0.005 (3)
β_1 magnitude (deg)	28.95	29.92		30.04
accuracy (±)	0.2			0.28
pitch variation (±)	0.47 (4)	0.13 (6)		0.13 (2)
Exit flow conditions:				
M_2 magnitude	0.933	0.957	0.828	0.932
accuracy (±)		0.003		0.004
pitch variation (±)	0.006 (3)	0.003 (4)	0.003 (3)	0.004 (2)
β_2 magnitude (deg)	67.03	67.02	67.33	67.76
accuracy (±)	0.2	0.4		0.3
pitch variation (±)	0.15 (3)	0.22 (4)	0.06 (3)	0.10 (2)
Overall:				
ξ magnitude	0.046	0.049	0.039	0.040
accuracy (±)		0.001		0.003
pitch variation (±)	0.007 (3)	0.001 (4)	0.003 (3)	0.003 (2)
Ω magnitude	0.929	0.937	0.984	1.012
accuracy (±)				0.029
pitch variation (±)	0.011 (3)	0.008 (4)	0.006 (3)	0.01 (2)

Table 4 Pitchwise variation of flow quantities in the inlet and exit planes, showing average values, periodicity and estimates of experimental accuracy. Numbers in parentheses indicate the number of pitches over which the averaging was done in each case.

Tunnel	M_1	Inlet duct length / Channel width
OX	0.252	3
BS	0.266	5
GO	0.282	20
RG	0.282	20

Table 5 Correlation of measured inlet Mach number for a choked cascade with tunnel inlet geometry

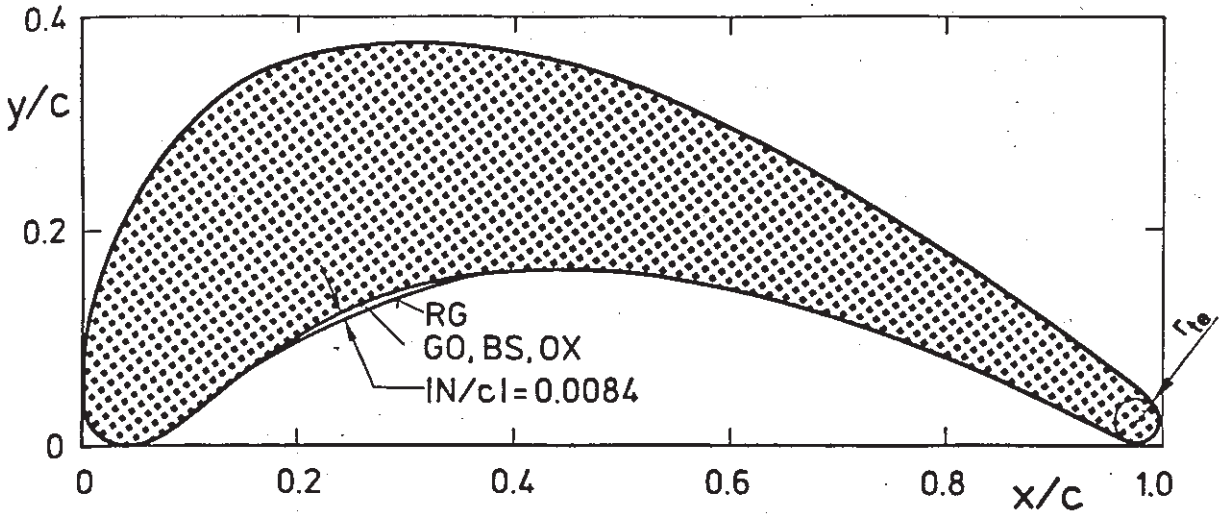

Fig. 1 The VKI-1 blade profile

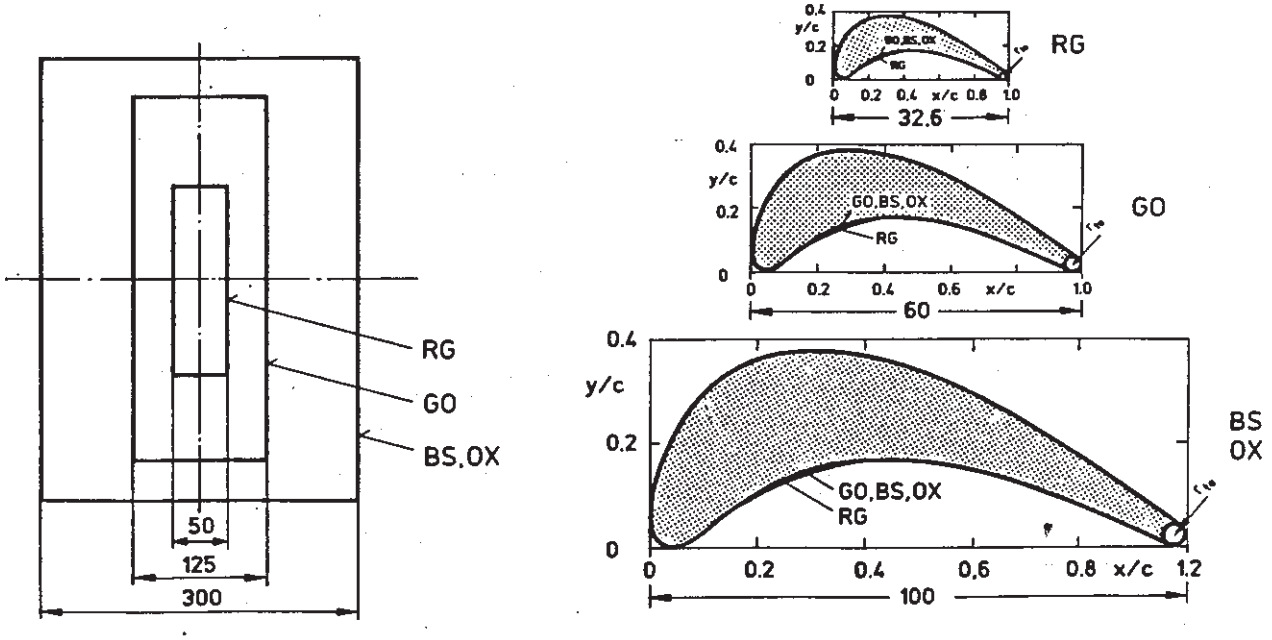

Fig. 2 Comparison of blade sizes in the four tunnels

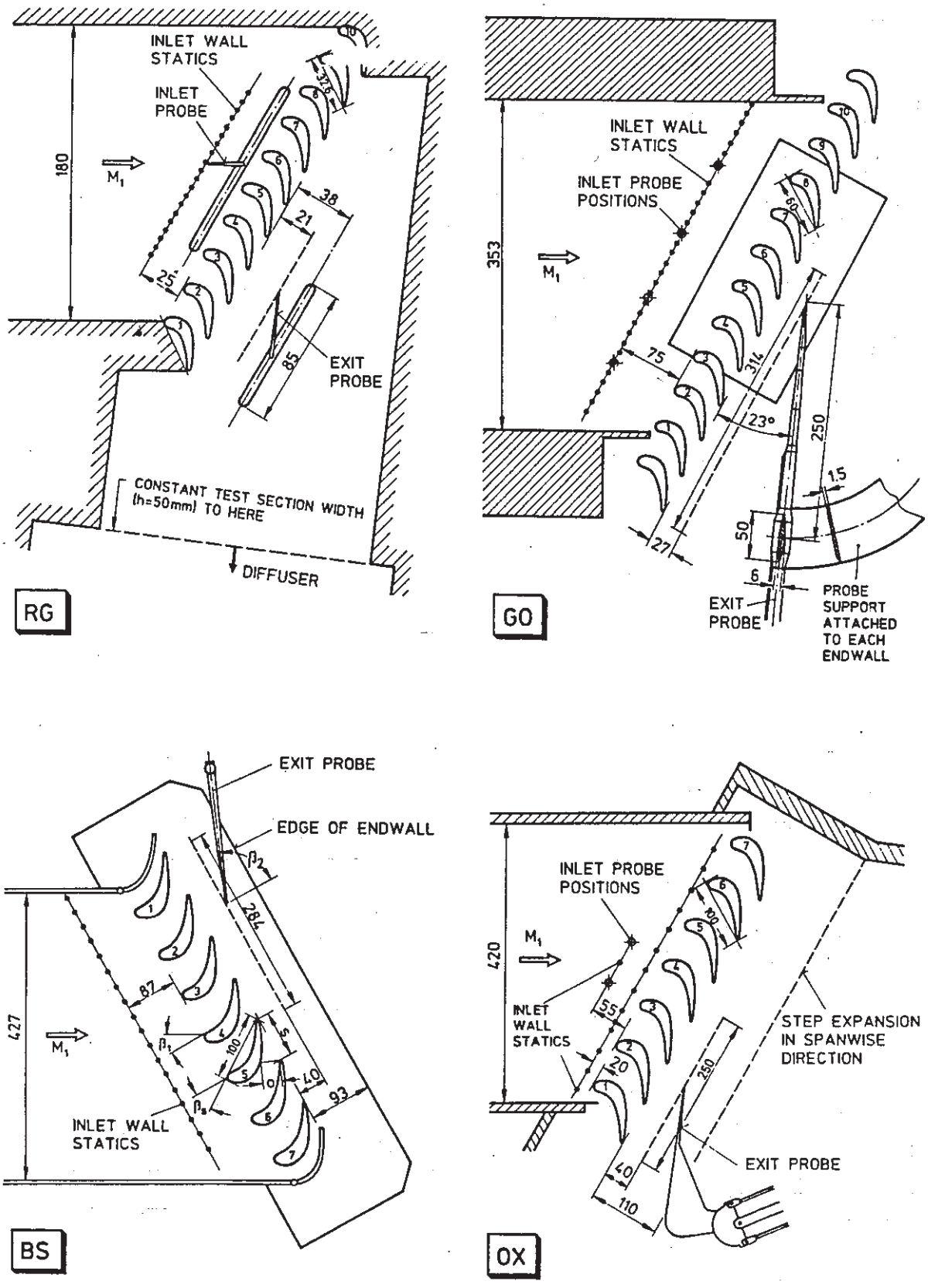

Fig. 3 Comparison of test sections

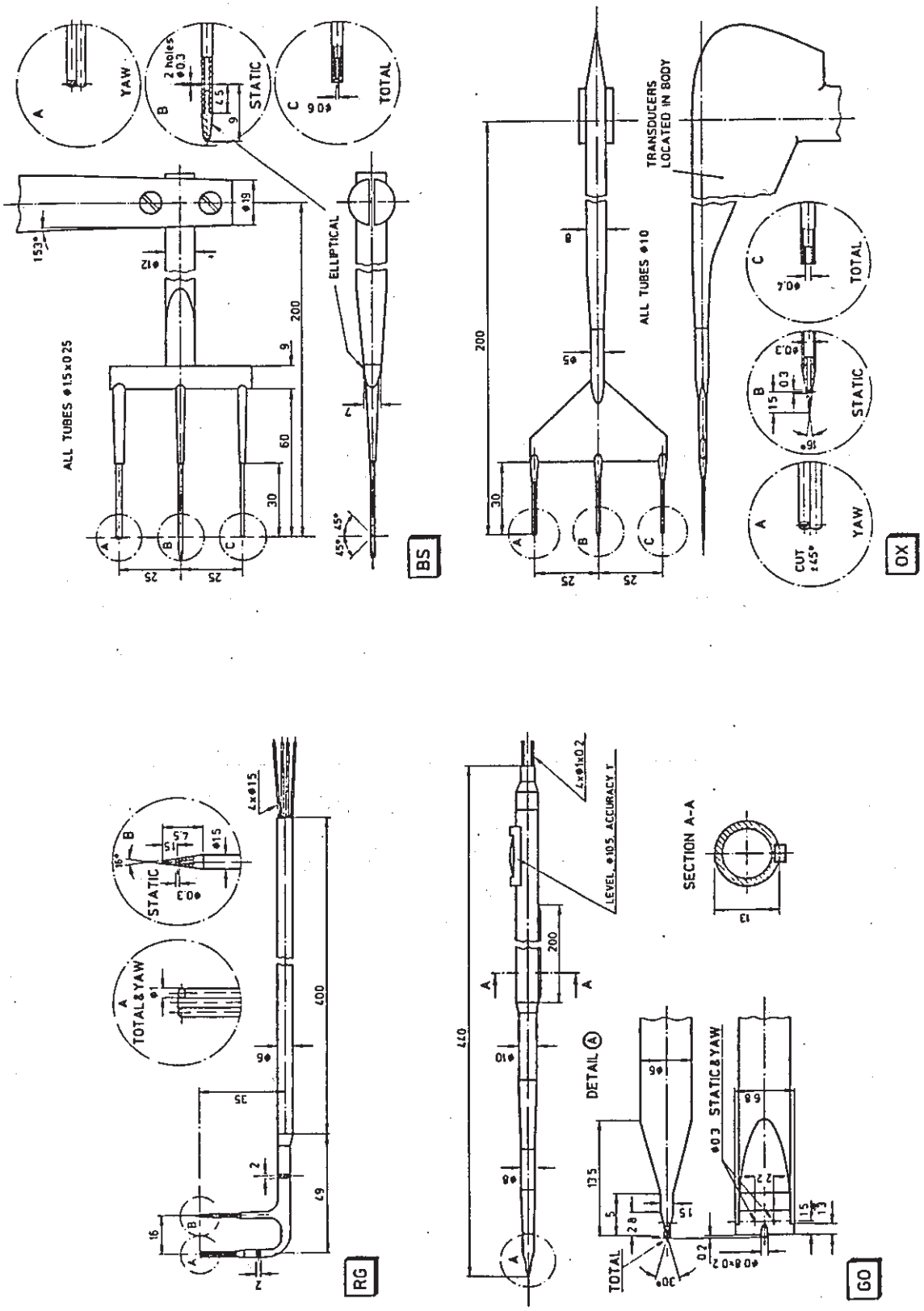

Fig. 4 Comparison of wake traverse probes

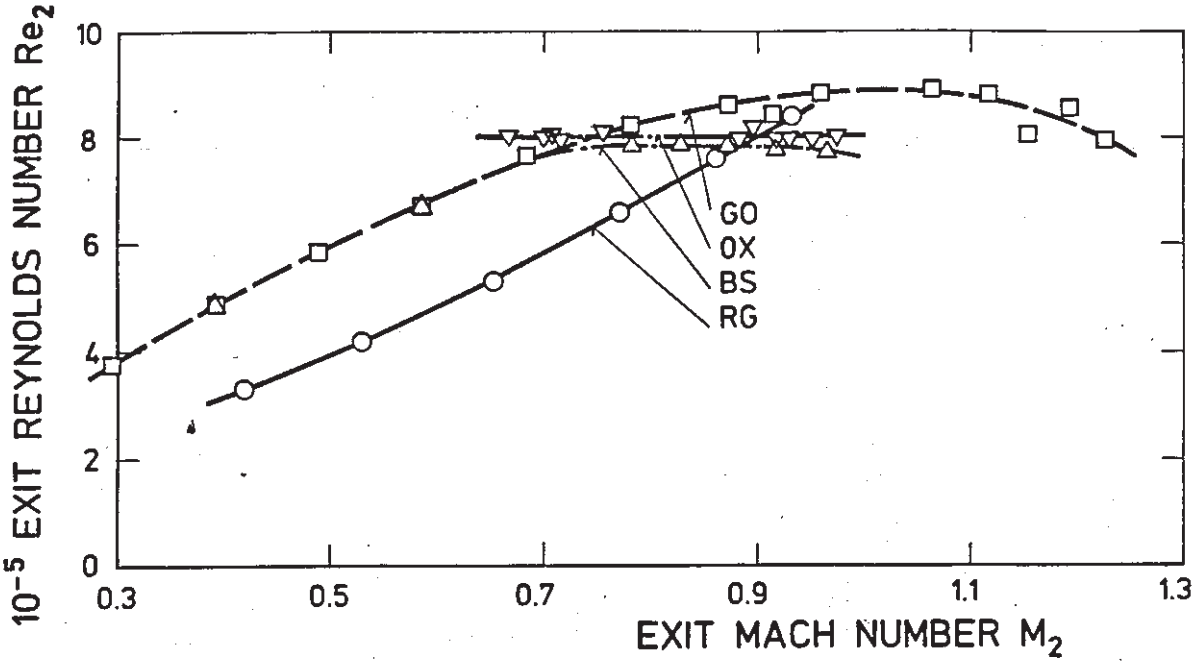

Fig. 5 Exit Reynolds number as a function of exit Mach number

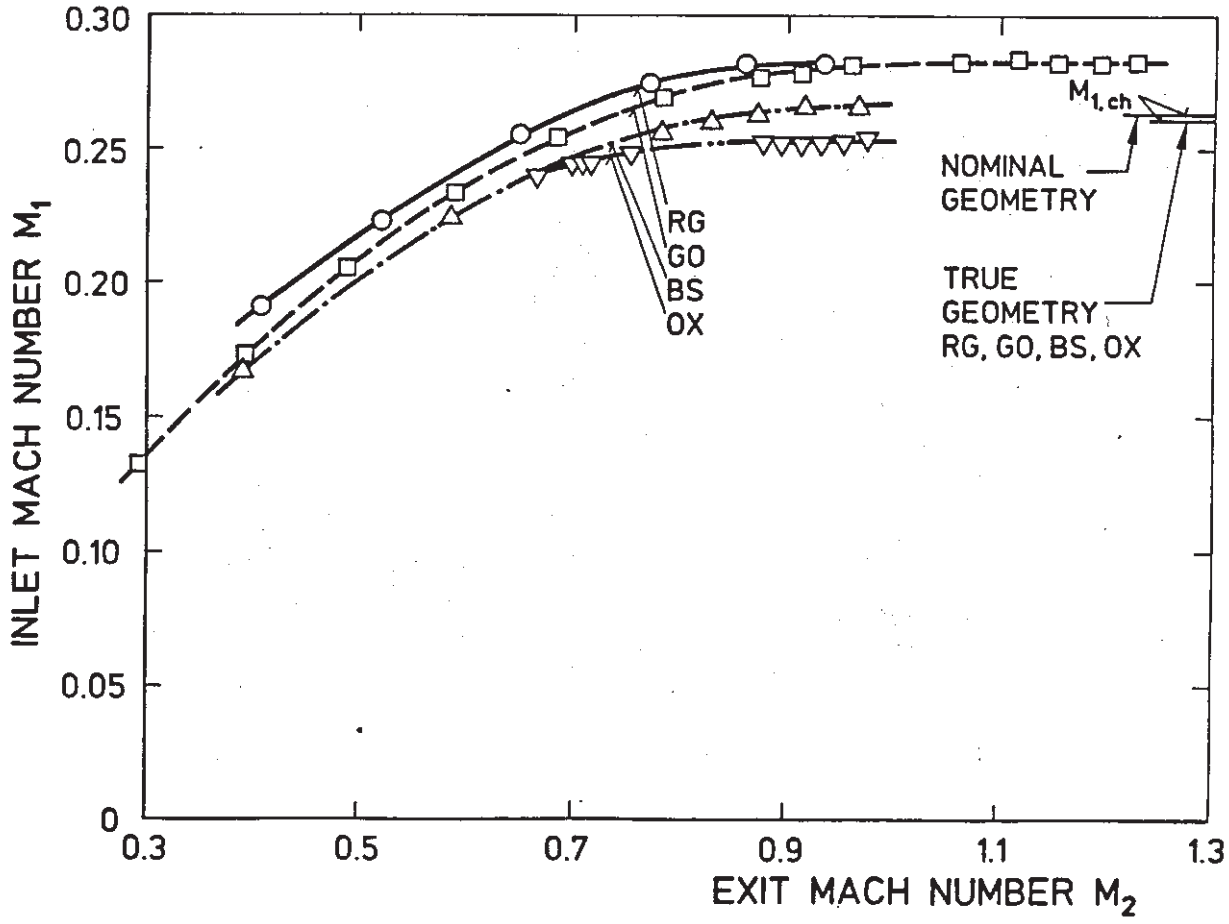

Fig. 6 Inlet Mach number as a function of exit Mach number

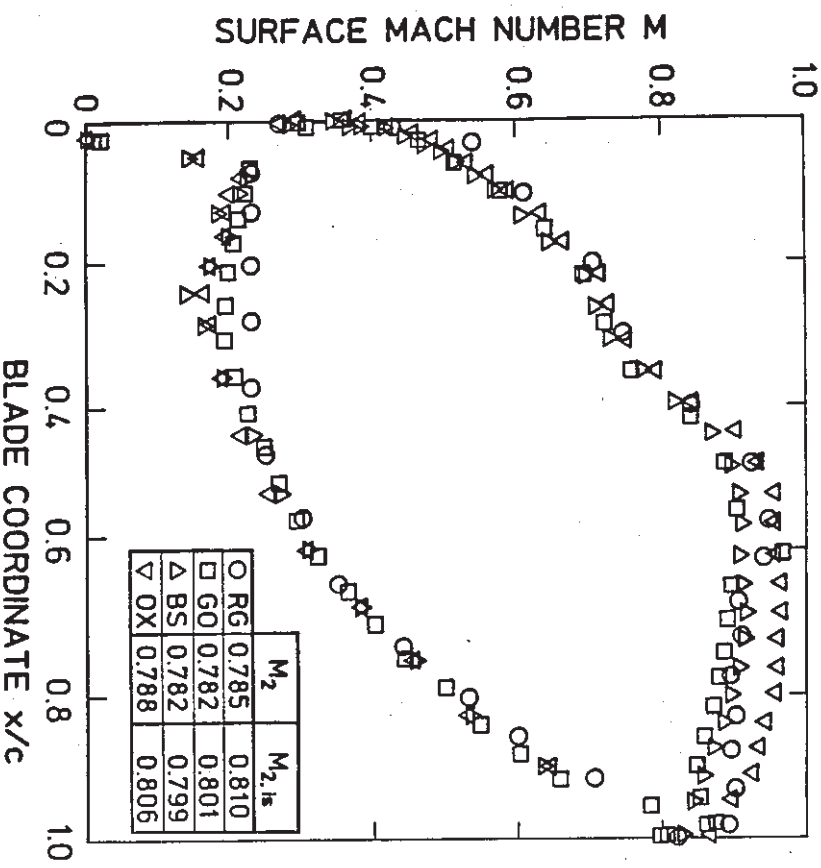

Fig. 7 Blade surface Mach number distribution, $\beta_1=30°$, $M_2=0.78$, $Re_2=6.8 - 8.2 \times 10^5$

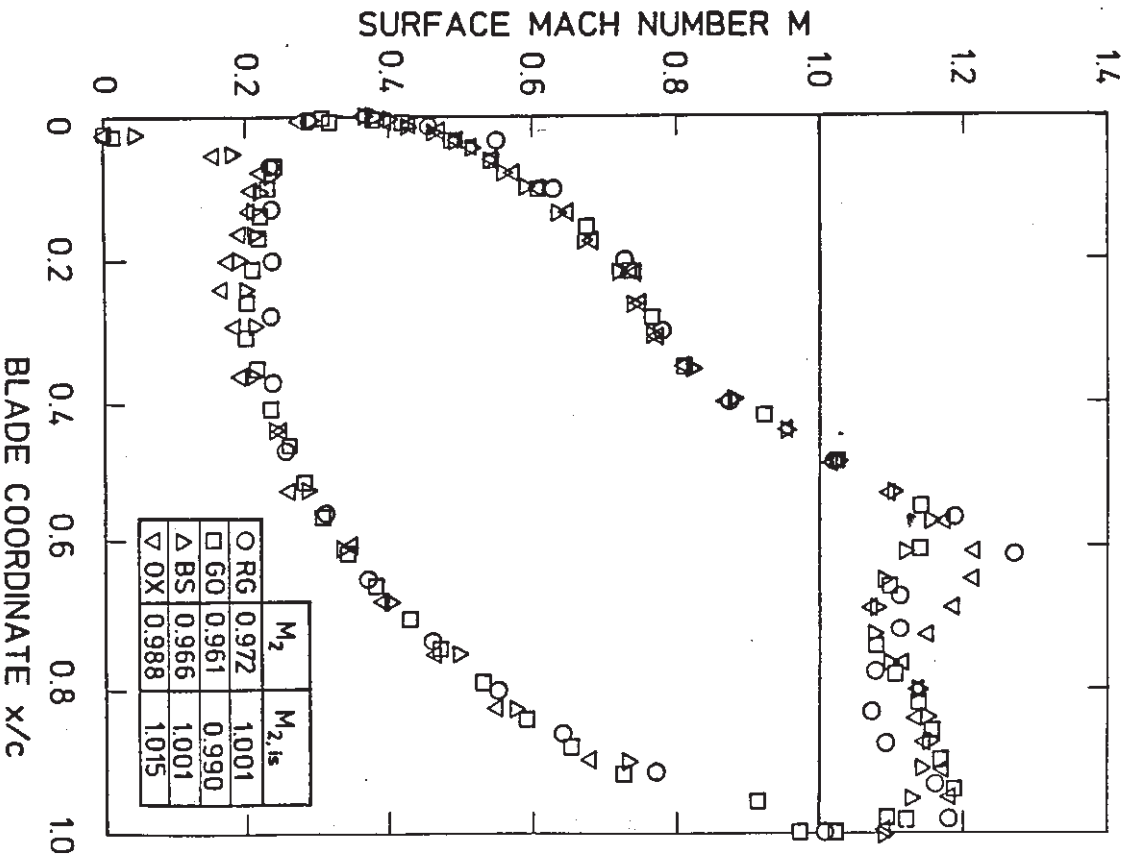

Fig. 8 Blade surface Mach number distribution, $\beta_1=30°$, $M_2=0.97$, $Re_2=7.6 - 8.9 \times 10^5$

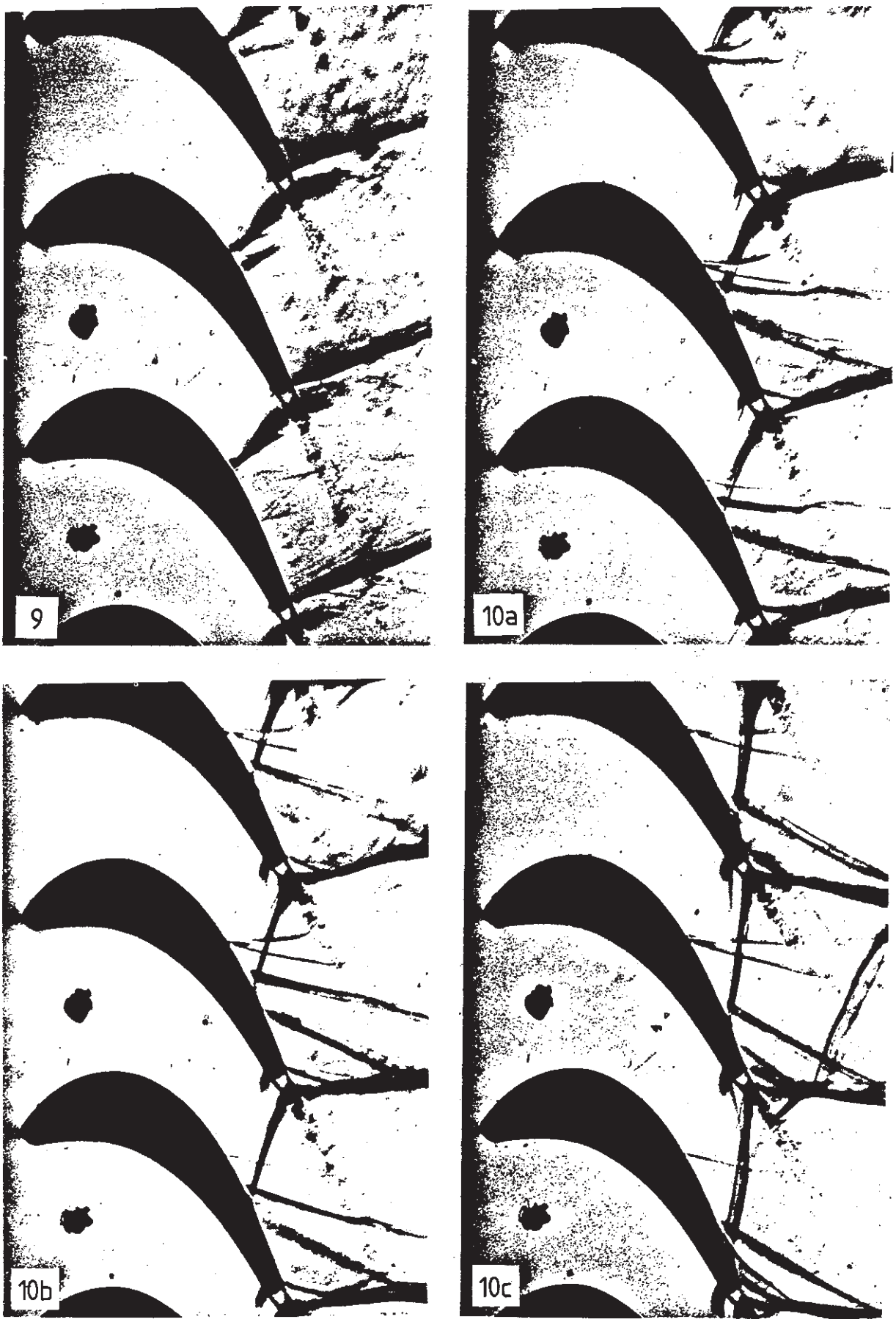

Fig. 9 Schlieren photograph from GO, $\beta_1 = 30°$, $M_2 = 0.96$, $Re_2 = 8.8 \times 10^5$

Fig. 10 Schlieren photographs from GO, $\beta_1 = 30°$, $Re_2 = 8.8 \times 10^5$
(a) $M_2 = 1.050$, (b) $M_2 = 1.133$, (c) $M_2 = 1.159$

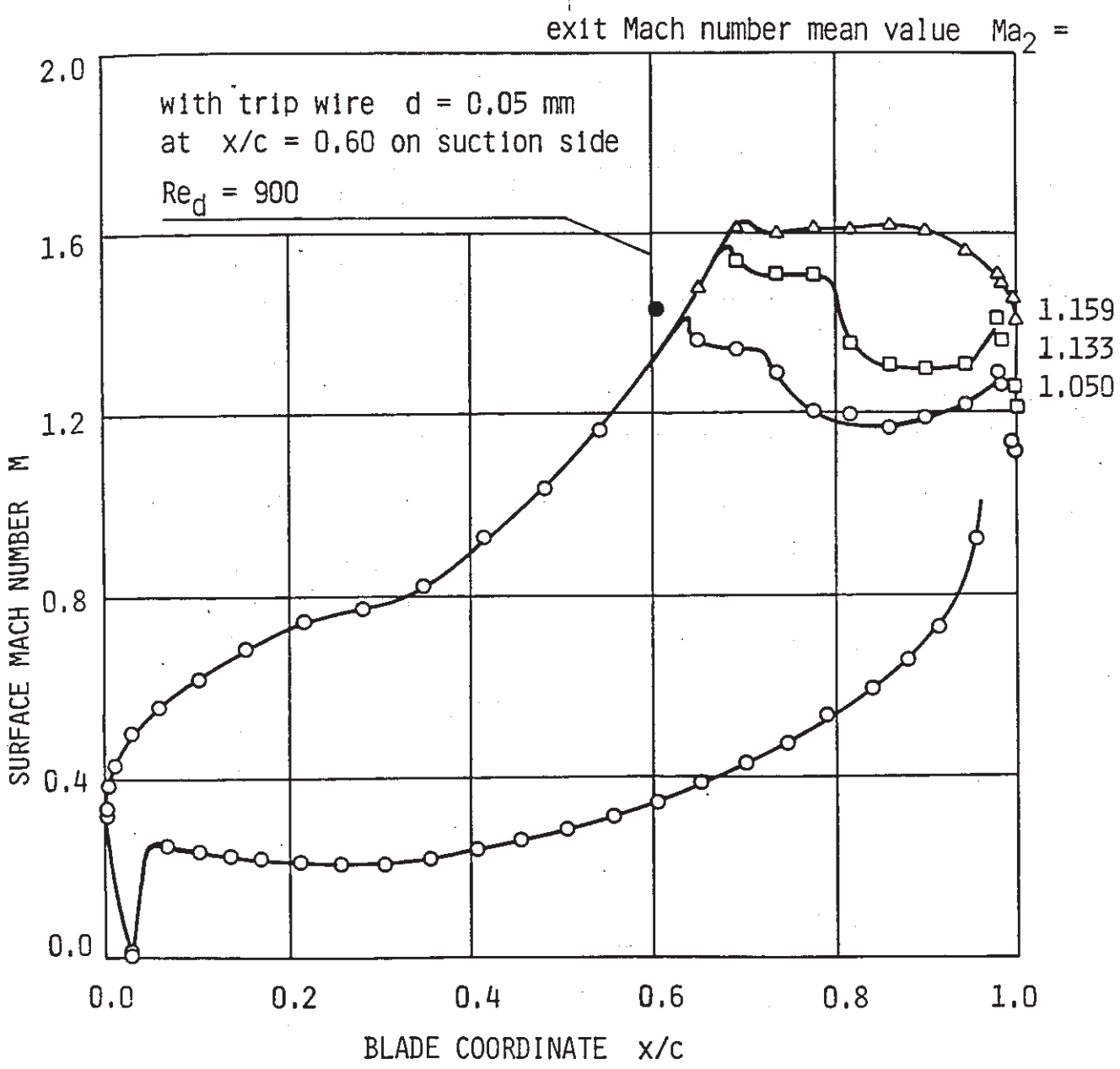

Fig. 11 Blade surface Mach number distribution for three supersonic exit Mach numbers, $\beta_1=30°$, $Re_2=8.8 \times 10^5$

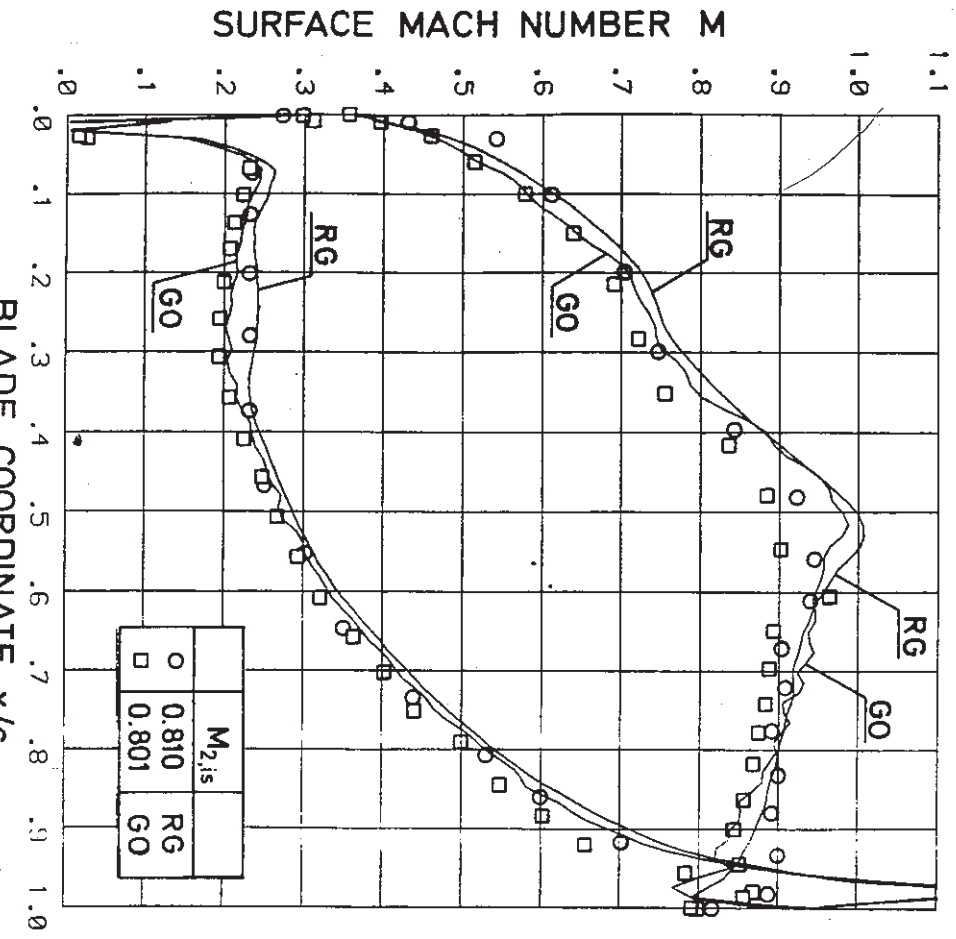

Fig. 12 Comparison of experimental measurements and theoretical predictions for RG and GO cascades - subsonic case

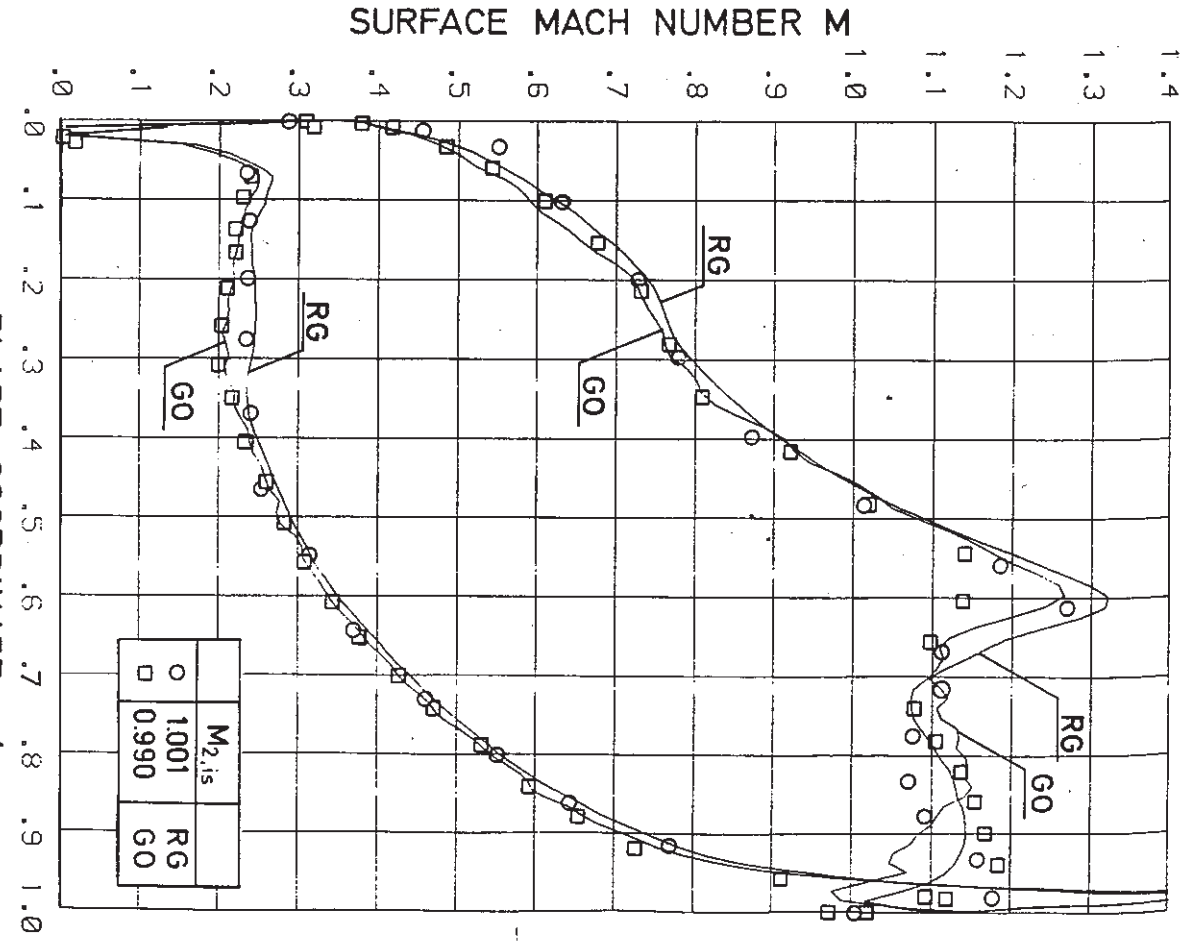

Fig. 13 Comparison of experimental measurements and theoretical predictions for RG and GO cascades - transonic case

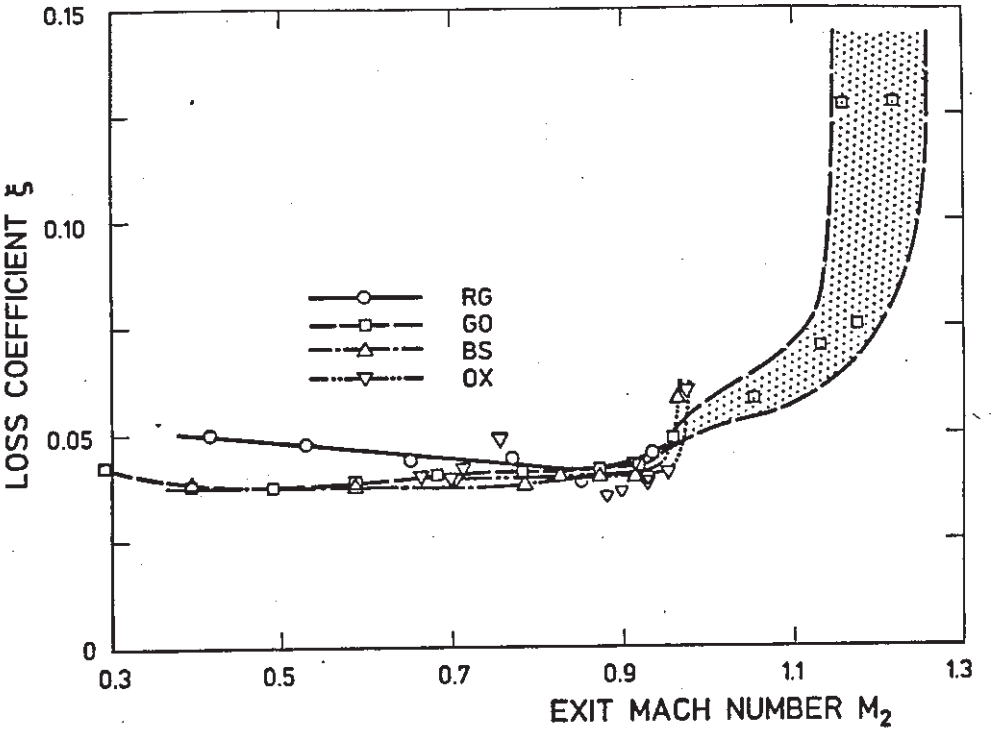

Fig. 14 Loss coefficient versus exit Mach number

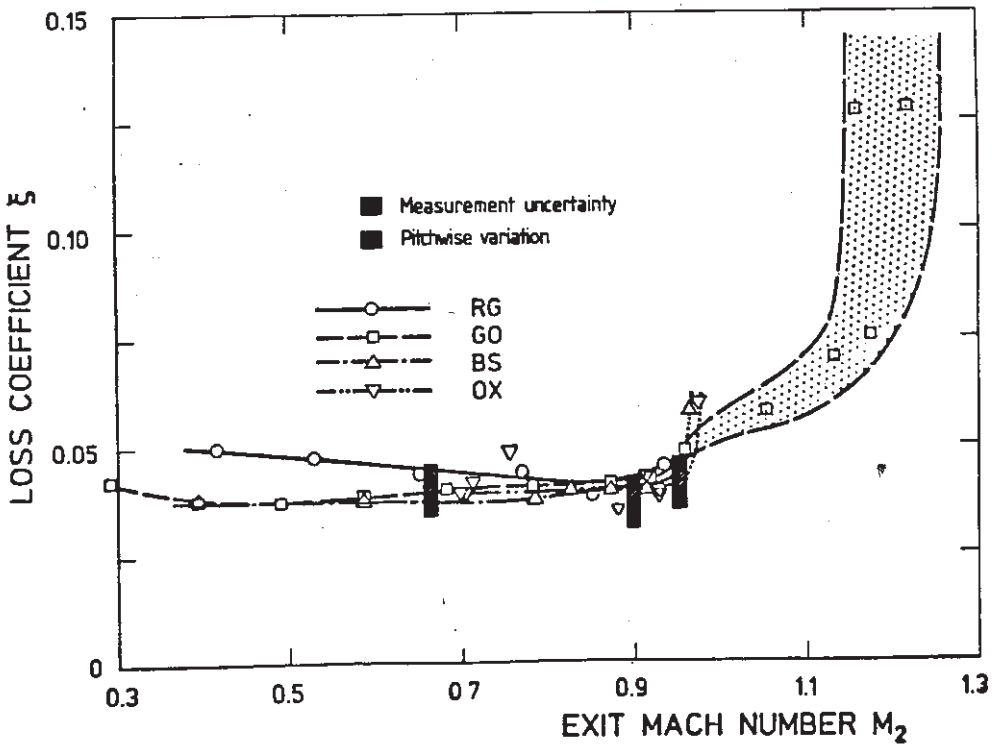

Fig. 15 Loss coefficient, showing the effect of pitchwise variation and measurement uncertainty at OX

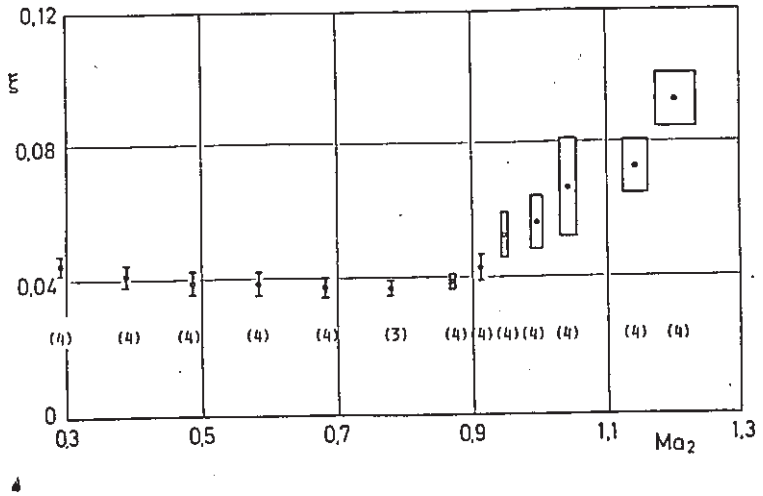

Fig. 16 Loss coefficients from GO, showing mean values and standard deviations for ( ) pitches - untripped case

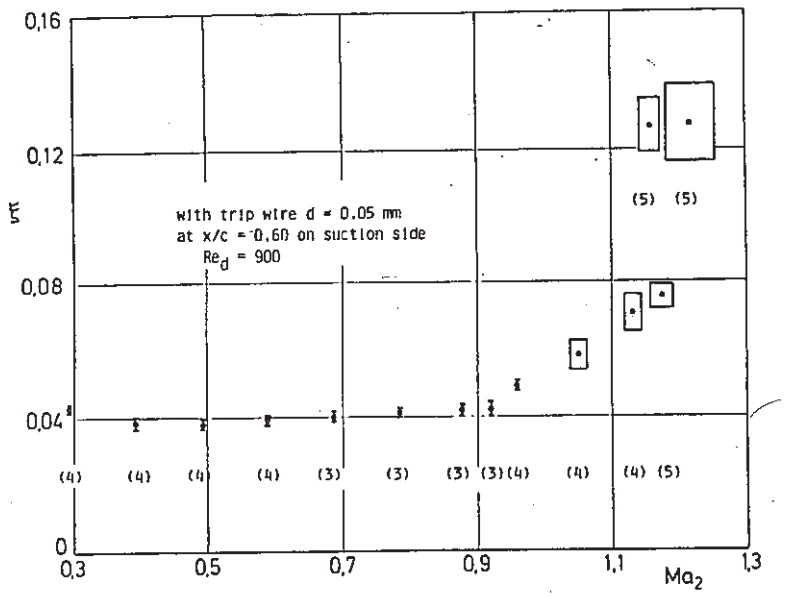

Fig. 17 Loss coefficients from GO, showing mean values and standard deviations for ( ) pitches - tripped case

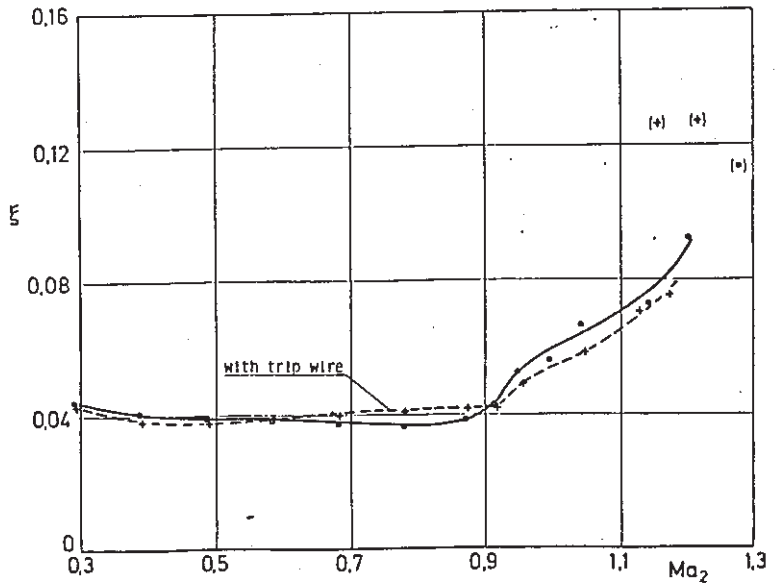

Fig. 18 Loss coefficients from GO, showing the effect of the trip wire on mean values

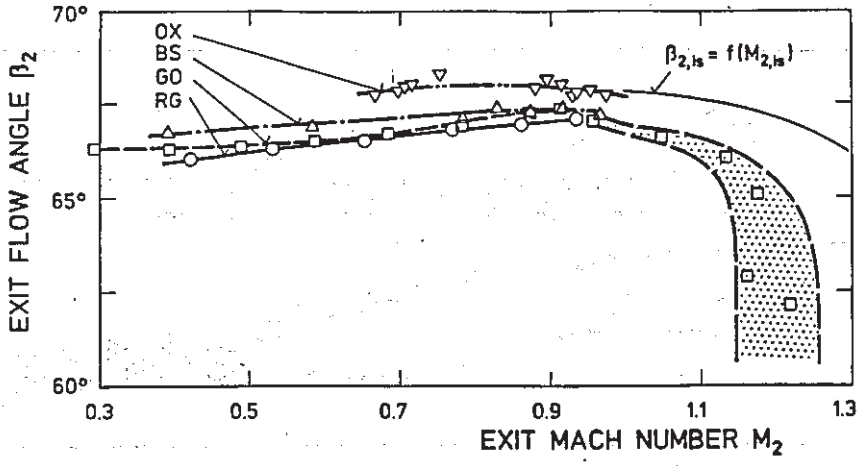

Fig. 19. Exit flow angle versus exit Mach number

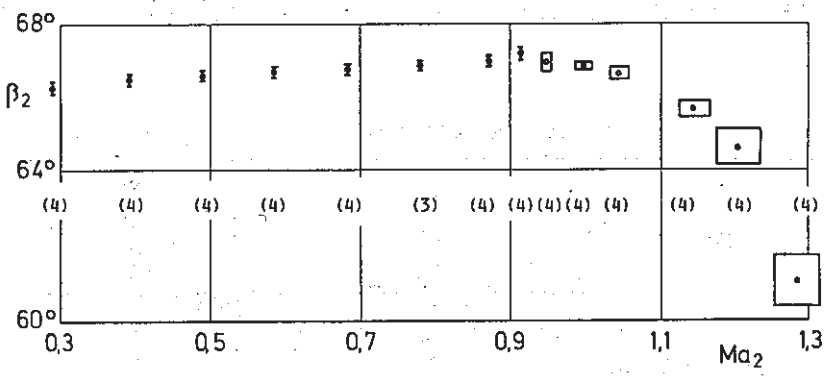

Fig. 20. Exit flow angle from GO, showing mean and standard deviations for ( ) pitches - untripped case

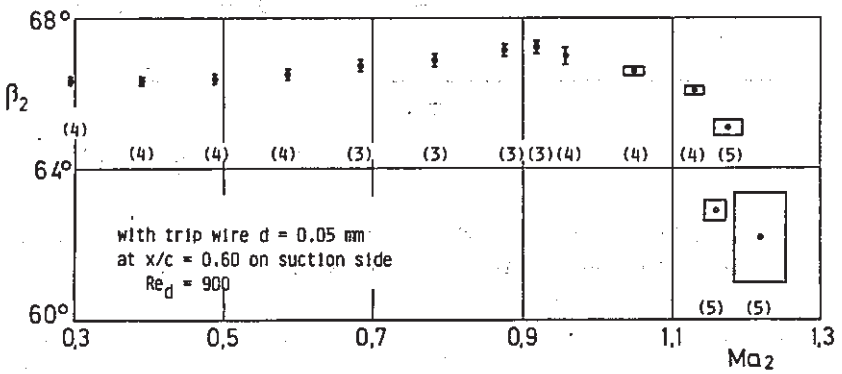

Fig. 21 Exit flow angle from GO, showing mean and standard deviations for ( ) pitches - tripped case

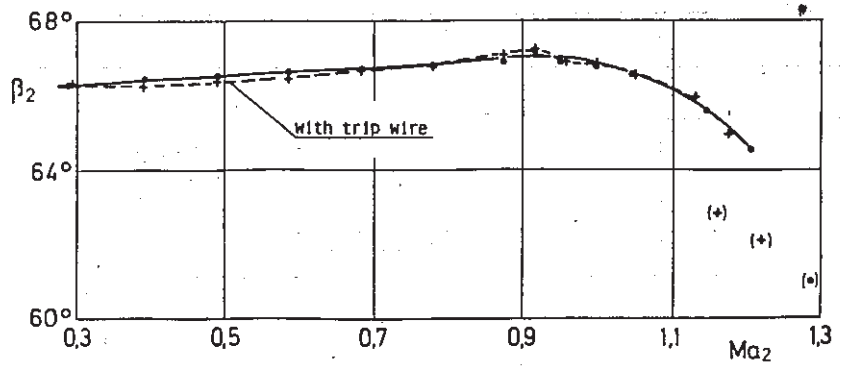

Fig. 22 Exit flow angle from GO, showing effect of the trip wire on mean values

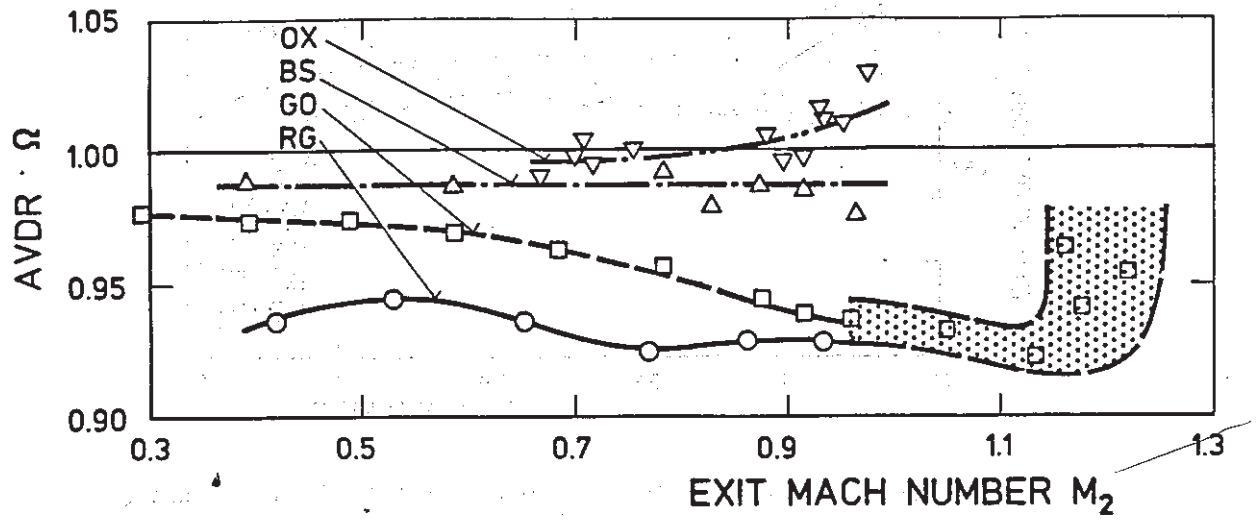

Fig. 23 Axial velocity density ratio versus exit Mach number

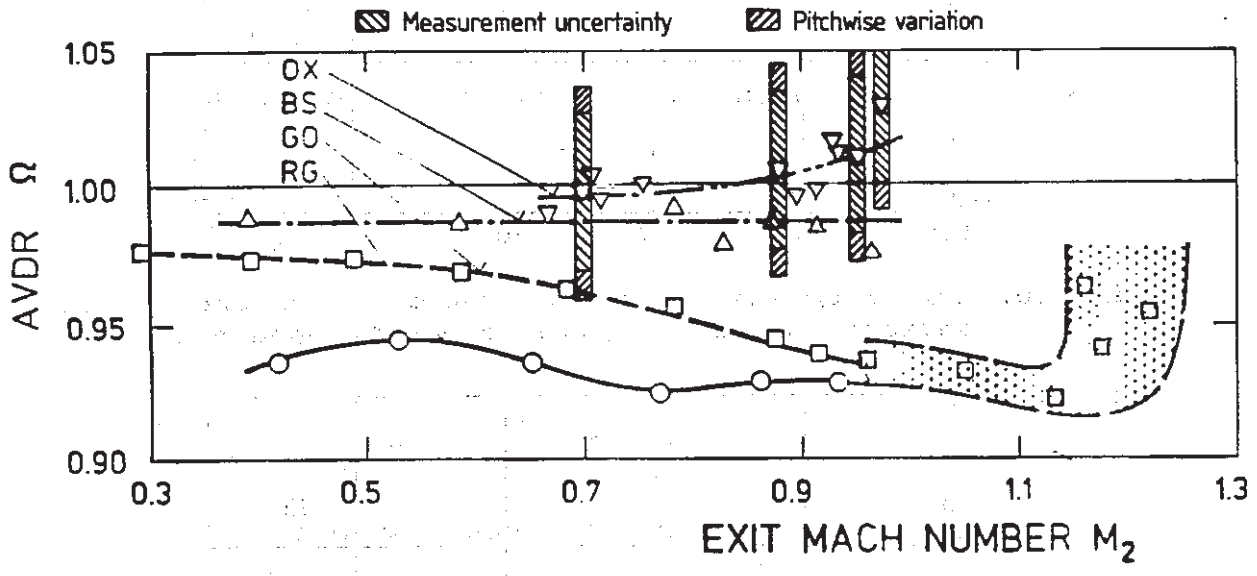

Fig. 24 Axial velocity density ratio, showing effects of measurement uncertainty and pitchwise variation

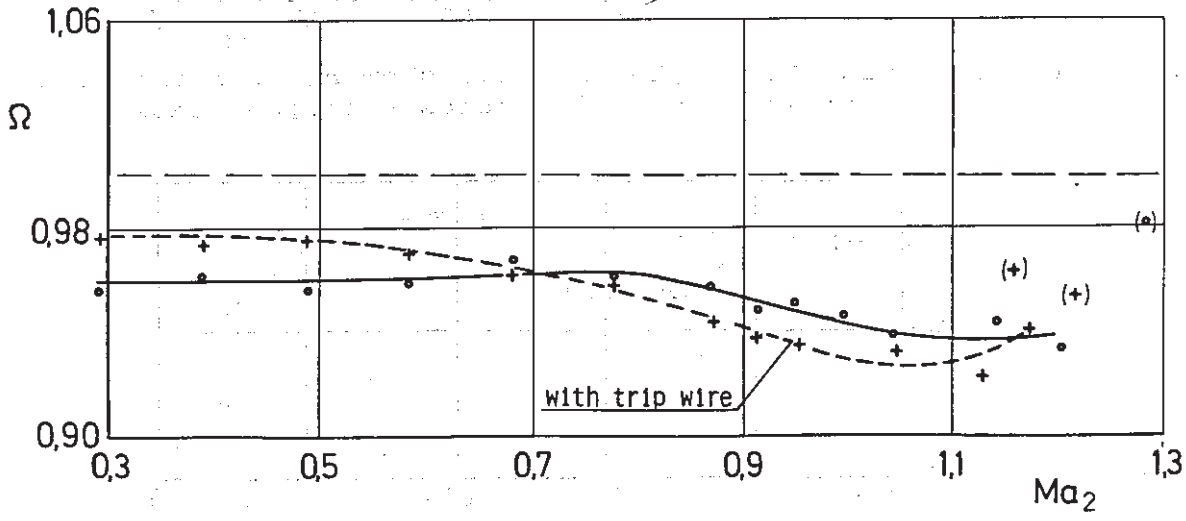

Fig. 25 Axial velocity density ratio from GO, showing effect of the trip wire on mean values

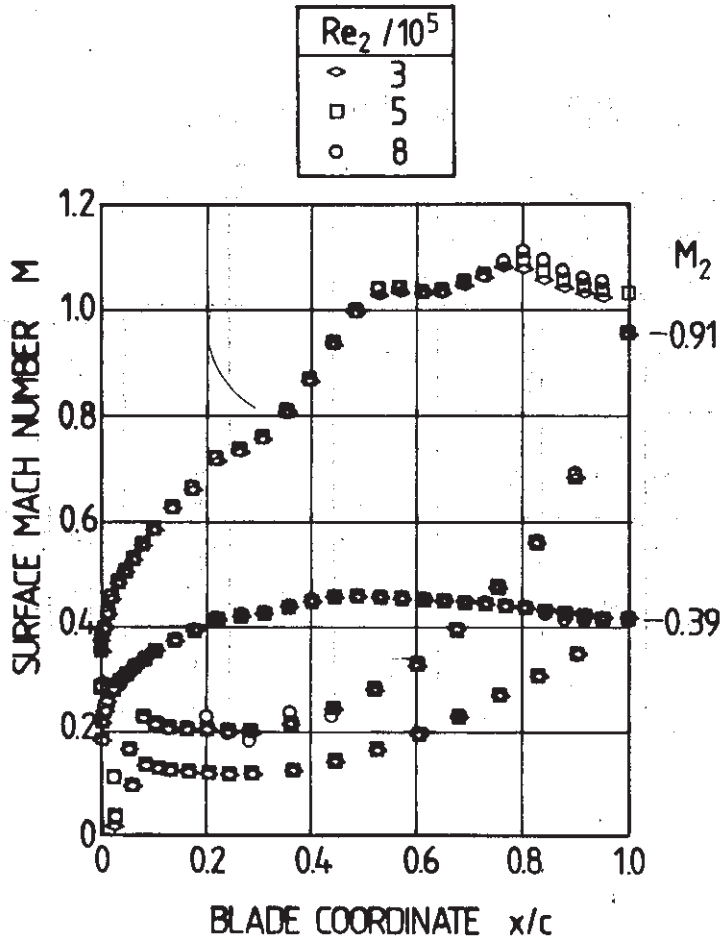

Fig. 26 Blade surface Mach number distributions of BS tunnel: influence of exit Reynolds and Mach numbers

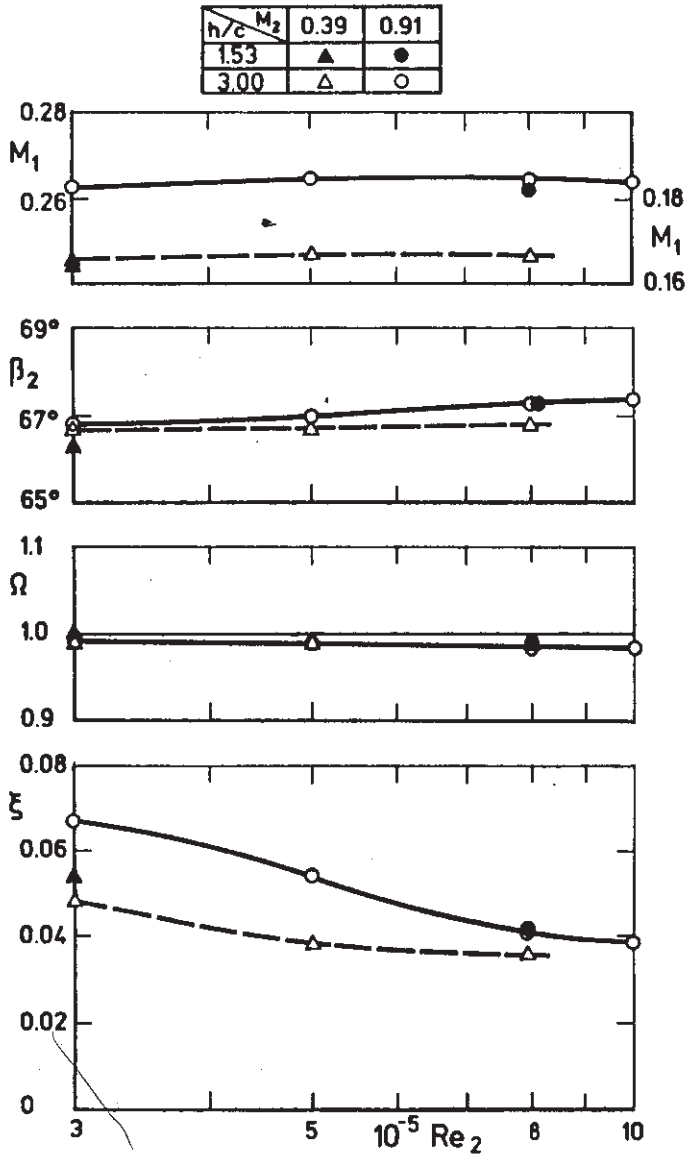

Fig. 27 Inlet Mach number and average wake traverse data of BS tunnel: influence of exit Reynolds and Mach numbers and aspect ratio h/c

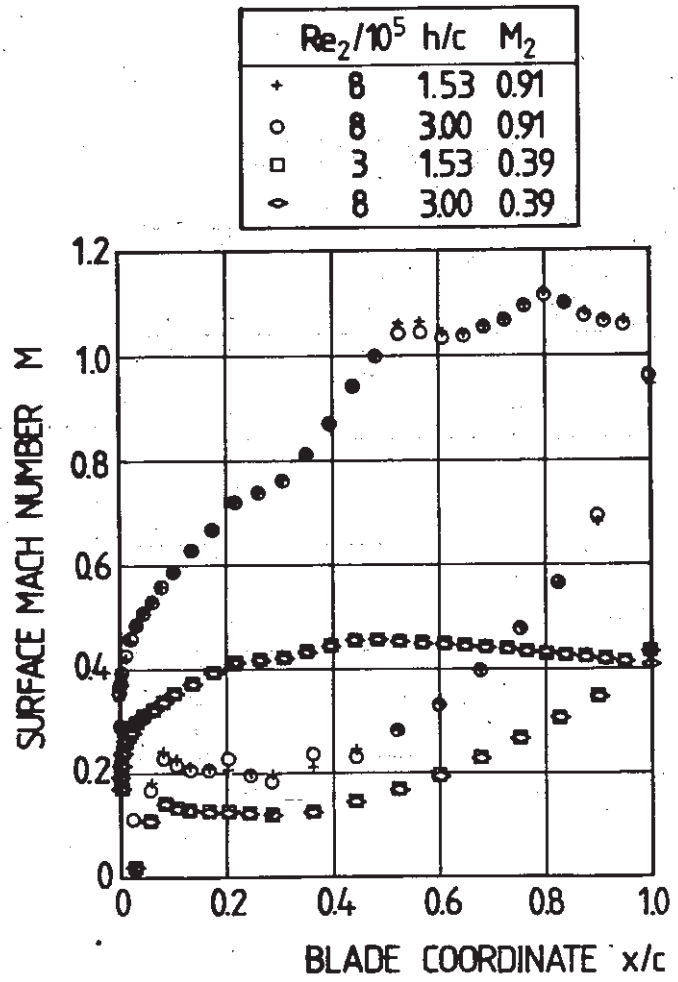

Fig. 28 Blade surface Mach number distributions of BS tunnel: influence of exit Reynolds and Mach numbers and aspect ratio h/c

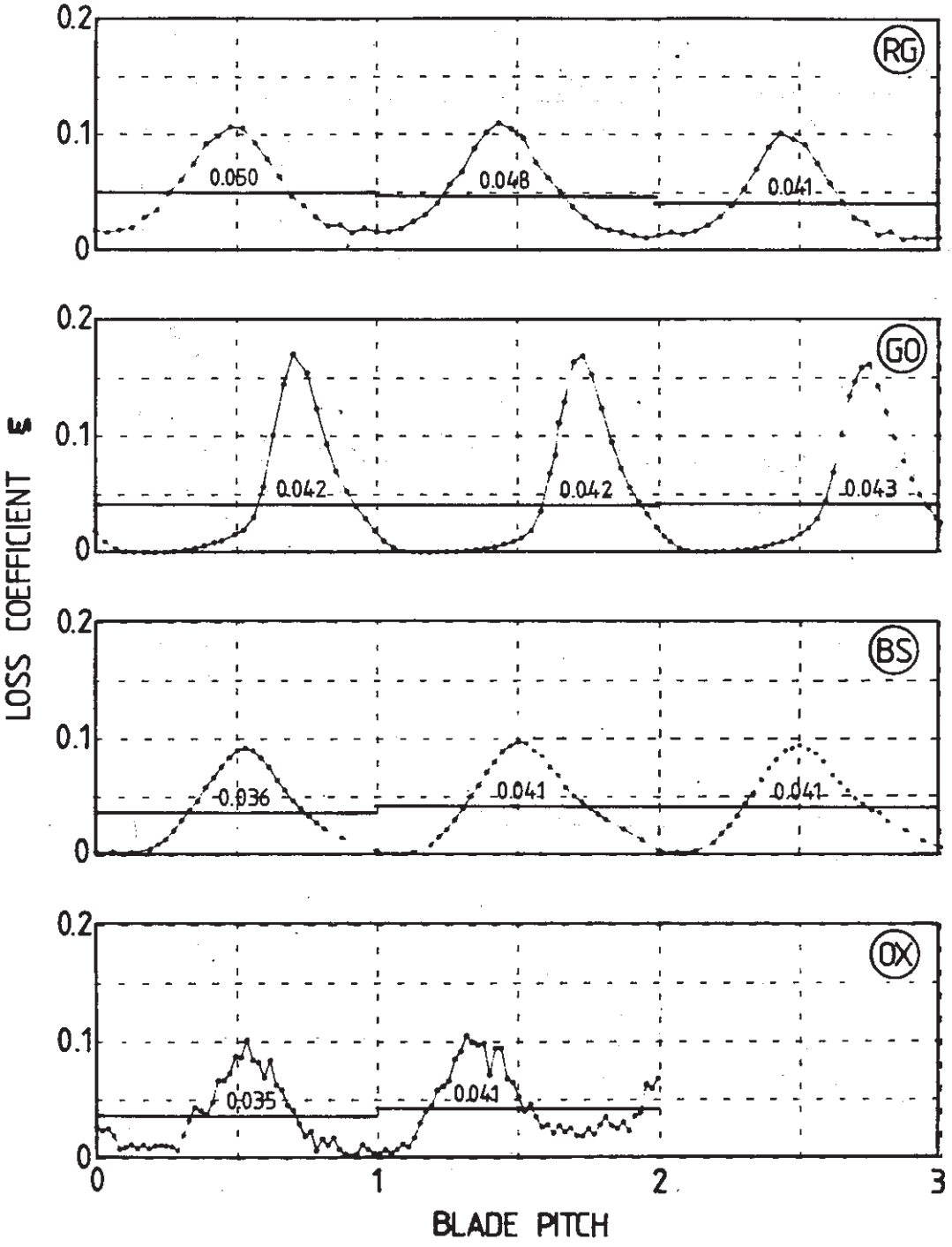

Fig. 29 Comparison of local wake measurements of loss coefficient, showing also average values for each pitch (RG, GO and OX: $M_2 \simeq 0.91$, BS: $M_2 \simeq 0.83$)

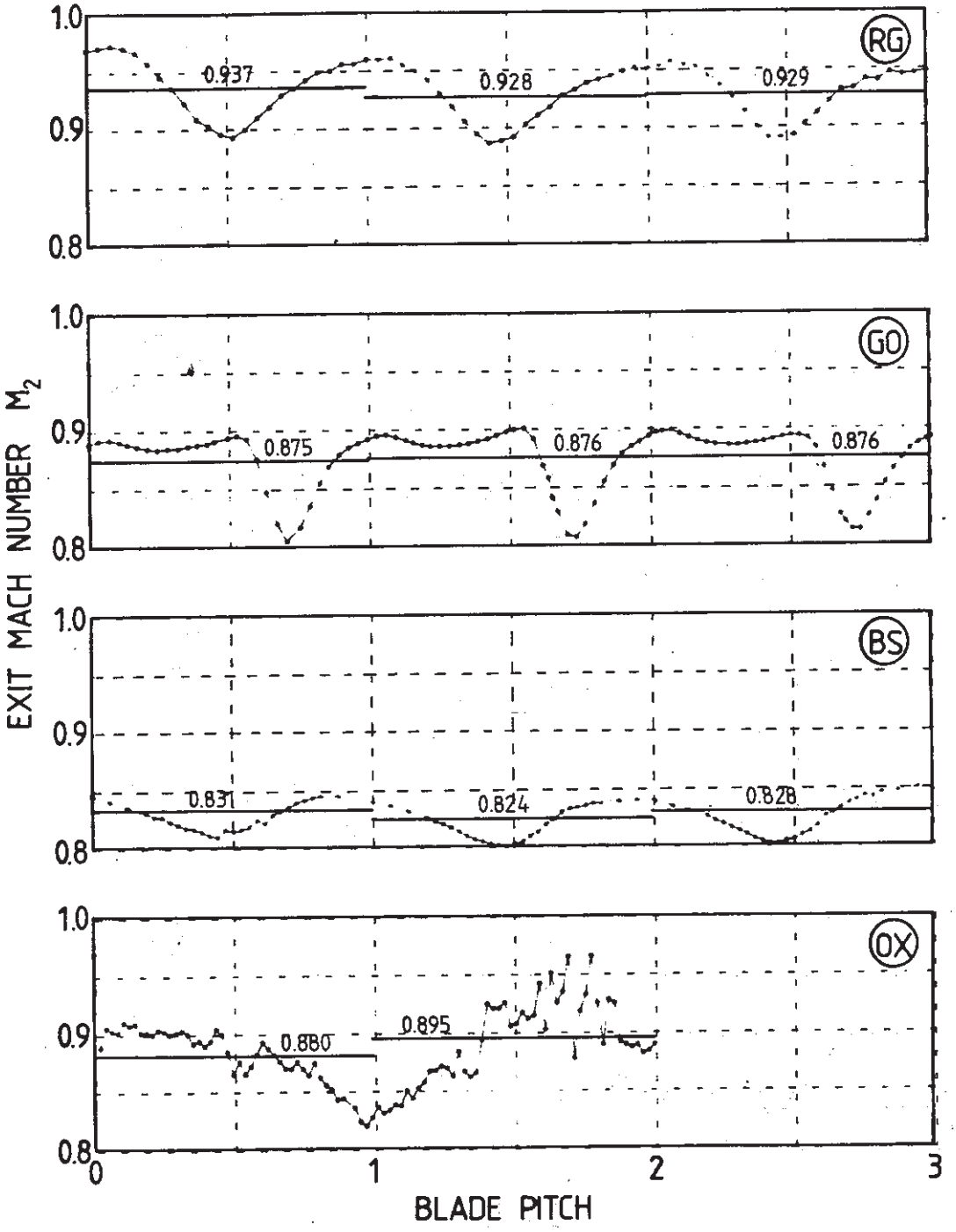

Fig. 30 Comparison of local wake measurements of exit Mach number, showing also average values for each pitch (RG, GO and OX: $M_2 \simeq 0.91$, BS: $M_2 \simeq 0.83$)

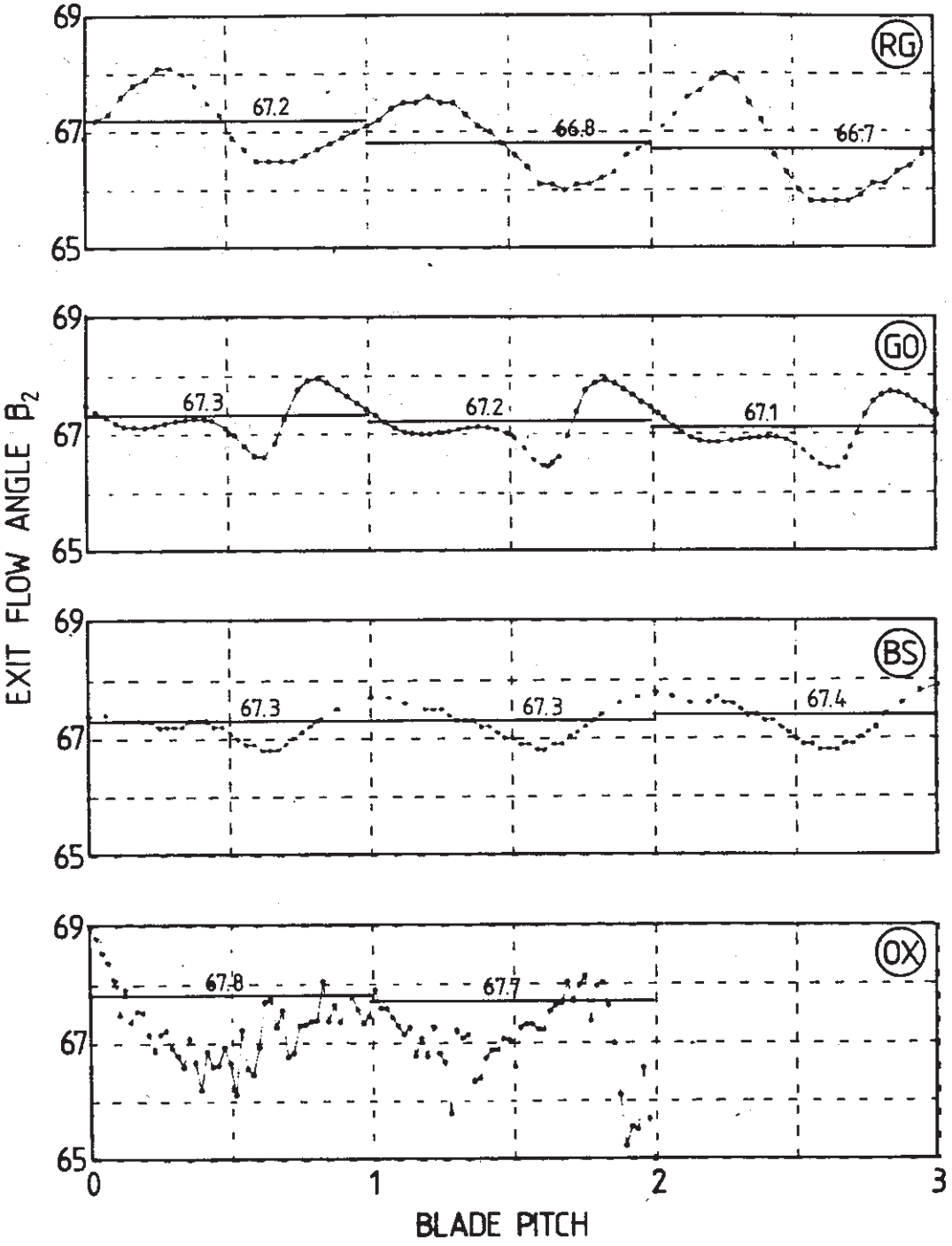

Fig. 31 Comparison of local wake measurements of exit flow angle, showing also average values for each pitch (RG, GO and OX: $M_2 \simeq 0.91$, BS: $M_2 \simeq 0.83$)

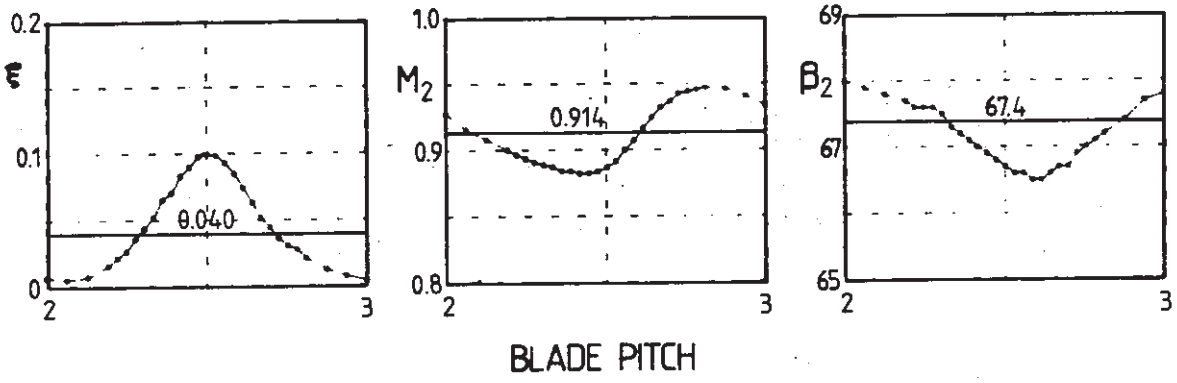

Fig. 32 Local wake measurements from BS at M_2 = 0.91, showing also average values. The pitch axis is scaled to be compatible with those used in Figures 29-31.

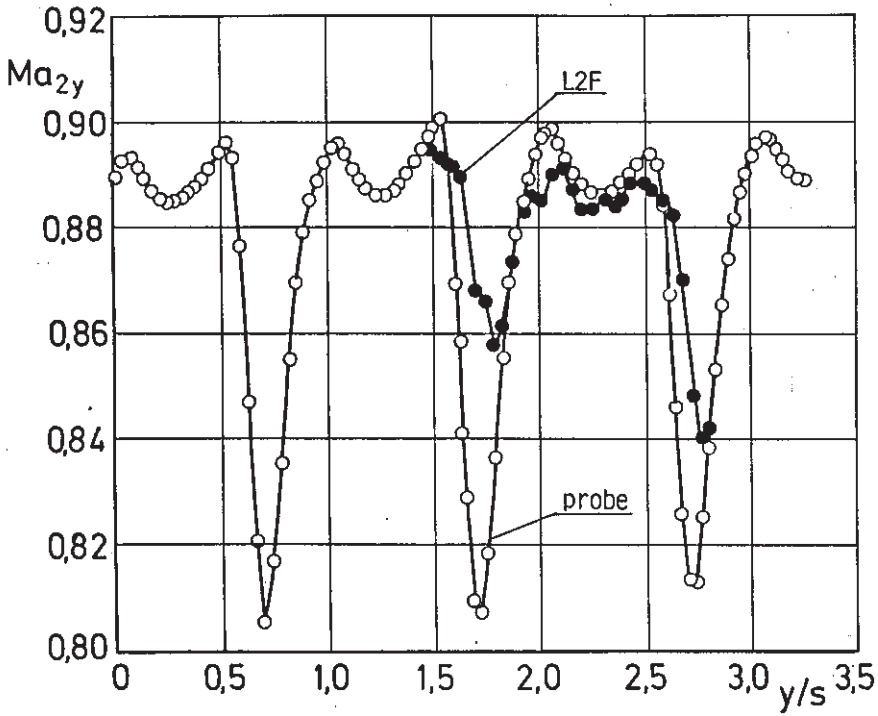

Fig. 33 Local exit Mach number distribution from GO: comparison of probe and L2F results

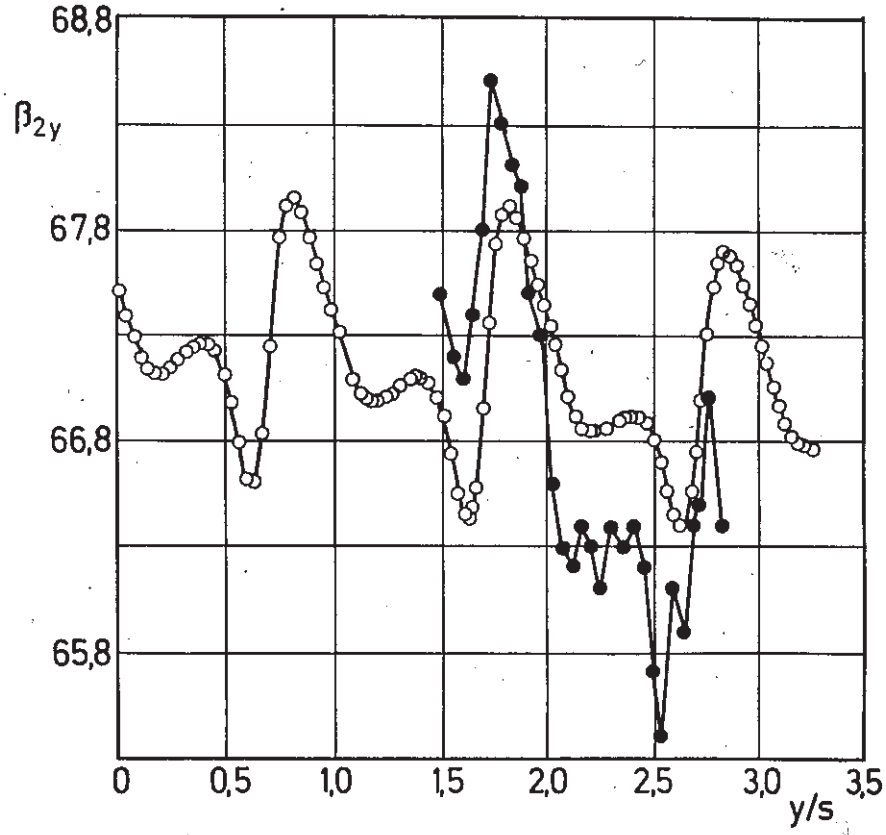

Fig. 34 Local exit angle distribution from GO: comparison of probe and L2F results